

JAMES COOK UNIVERSITY
COLLEGE OF SCIENCE &
ENGINEERING

EG4012
Civil Engineering

**THE EFFECTS OF NOTCHING ON
RECTANGULAR AND ROUND
TIMBER GIRDERS**

LARA MULLAMPHY

THESIS SUBMITTED TO THE COLLEGE OF SCIENCE & ENGINEERING IN PARTIAL
FULFILMENT OF THE REQUIREMENTS FOR THE DEGREE OF
**BACHELOR OF ENGINEERING
(CIVIL ENGINEERING)**

7 OCTOBER 2016

Statement of Access

I, the undersigned, author of this work, understand that James Cook University may make this thesis available for use within the University Library and, via the Australian Digital Theses network, for use elsewhere. I understand that, as an unpublished work, a thesis has significant protection under the Copyright Act and I do not wish to place any further restriction on access to this work.

Signature

Date

Declaration of Sources

I declare that this thesis is my own work and has not been submitted in any form for another degree or diploma at any university or other institution of tertiary education. Information derived from the published or unpublished work of others has been acknowledged in the text and a list of references is given.

Signature

Date

Abstract

This thesis describes the background, methodology, results, discussion and conclusions for a civil engineering undergraduate project. This is given in five chapters with the overall objective of this thesis is to obtain a greater understanding of the behaviour of the cracking and eventual failure of notched timber beams commonly used in railway bridge construction.

A background study was carried out on current timber bridge construction in Australia including the types of timbers used, deterioration, shear and flexural cracking and ultimate beam failure. Types of notching currently in use are also discussed as well as forms of potential beam reinforcement to reduce the likelihood of potential cracking and ultimate failure.

Experiments were carried out on twelve rectangular section and twelve round section notched timber members. These members were placed under a steadily increasing central load and observed for initiation of notch cracking, crack propagation and ultimate failure. The rectangular and circular specimens were each separated into three groups of notch slopes 1:0, 1:2 and 1:4 and observations were taken on the time and position of crack initiation, direction of crack propagation, time between crack initiation and ultimate failure and type of ultimate failure.

After initiation, the cracks all propagated along the direction of the timber grain with the rate of notch crack growth occurring more rapidly in the rectangular specimens than round ones. The round specimens predominantly ultimately failed due to flexure while the rectangular specimens consistently failed in shear. The results showed that the critical notch slope was 1:0 for both the rectangular and round members, while the highest member capacities consistently occurred for the 1:4 notch.

Finally, a study of optimum design methods for the rectangular specimen was carried out by comparing the theoretical and measured capacities. The results showed that the AS1720 notch design and the CSA 0.86 gave poor agreement between the theoretical and experimental while the results obtained for Eurocode and AS1720 ultimate design yielded significantly better agreement. The optimum design method appears to be the AS1720 ultimate design for shear and bending, using the cross section over the notch. However this does not take into account notch slope and only designs for the beams ultimate failure, so the optimum design that accounts for notch crack initiation is the Eurocode 5 design. The AS1720 ultimate design in shear and bending method was modified to account for a notched circular section, and thus

a method of designing for a notched round beam was established. This method was also found to be relatively accurate, when compared to the experimental results.

Overall this thesis provides a greater understanding of the behaviour of cracking in notched beams for both rectangular and circular section members. The initiation and propagation of these cracks for differing notch slopes, combined with the results on ultimate beam failure, will provide valuable information which can be used in the optimum design for notched timber beams used in bridge construction.

Acknowledgements

First and foremost I would like to express my sincerest gratitude to my thesis supervisor, Associate Dean Rabin Tuladhar, whose knowledge, patience and guidance were invaluable to me.

I would also like to thank Justin Dewey, for the many stimulating discussions, answering all my questions and being so available to me, I am very grateful to have been able to work with you. My sincere thanks to our laboratory technician, Troy Poole, who was never disheartened no matter how many things went wrong or what equipment we broke. I thank my thesis partner, Lucy McCormack, for consistently keeping us on the same page and being so great to work with.

Lastly, I would like to give my sincerest thanks to my parents who have had to read many drafts and now know more about notched timber girders than they'd like to admit.

Contents

Statement of Access	ii
Declaration of Sources	iii
Abstract	iv
Acknowledgements	vi
List of Figures	xii
List of Tables	xii
1 Introduction	1
1.1 Objectives	2
1.2 Scope	2
2 Literature Review	3
2.1 Timber Bridges	3
2.1.1 Wood Types	4
2.1.2 Common Defects and Failures	5
2.2 Timber Properties	9
2.3 Australian Member Design	11
2.3.1 Rectangular Section	12
2.3.2 Circular Section	13
2.3.3 Octagonal Section	13
2.4 Notching	14
2.4.1 Notch Types	15
2.4.2 Notch Design	16
2.5 Timber Strengthening	21
2.5.1 Strengthening of Notched Beams	21
2.6 Analysis and Modelling	23
3 Materials and Methodology	25
3.1 Preliminary Results	25
3.1.1 Finite Element Analysis	25
3.2 Experimental Set-up	27
3.2.1 Altering Notch Angles of Small Scale Members	34

3.3	Material Properties	36
4	Results and Discussion	38
4.1	Rectangular Specimens	38
4.1.1	Loading Rates	38
4.1.2	Failure Modes	39
4.1.3	Ultimate Capacities	44
4.1.4	Strain Gauge Analysis	47
4.2	Round Specimens	57
4.2.1	Loading Rates	57
4.2.2	Failure Modes	58
4.2.3	Ultimate Capacities	63
4.2.4	Strain Gauge Analysis	65
4.3	Comparison of Round and Rectangular Section	72
4.4	Predicted Capacities using Standards	74
4.4.1	AS1720 Notch Design	74
4.4.2	Eurocode 5 Notch Design	75
4.4.3	CSA O.86 Notch Design	76
4.4.4	AS1720 Ultimate Section Design	77
4.4.5	Comparison of Design Methods	81
5	Conclusions	83
6	Recommendations	84

Appendix A *Rectangular Specimen Characteristics*

Appendix B *Round Specimen Characteristics*

Appendix C *Strain Gauge Results*

List of Figures

1	Wood Cell Structures	4
2	Weathering	6
3	Core and Notch Rotting	6
4	Locations of Flexural Cracking or Crushing	8
5	Locations of Shear Cracking	8
6	Standard Stress-Strain Diagram of Timber	9
7	Shear Stress Distribution	11
8	Notch Cracking	14
9	Member failure in bending over support	14
10	Fracture Modes (a) mode 1 (b) mode 2 (c) mode 3	15
11	Notching Types; (a) rectangular end notch; (b) tapered end notch; (c) rounded end notch; (d) notch in span	15
12	Notation for Notch	17
13	Geometry of notched beam and dowel joint	18
14	(a) Parameters of internal reinforcement (b) The theoretical portion of the shear stress taken by the reinforcement	22
15	TMR Standard Bolt Layout	22
16	Straps on Piles	23
17	Wood Axes	23
18	Properties used for ANSYS simulation	26
19	Rectangular Section Beam: deflection	26
20	Rectangular Section Beam: XY-plane shear strain	27
21	Rectangular Section Beam: normal strain in Y-direction (top) and Z-direction (bottom)	27
22	Rectangular Member Test Set-Up	28
23	Round Member Test Set-Up	29
24	Loading and LVDT Plate for Round Specimen	30
25	Strain Gauge and LVDT Layout	31
26	Set-up of loading plates, metal ball and load cell in MTS Machine	32
27	Notch Profiles for Rectangular Section Members	34
28	Notch Profiles for Circular Section Members	35
29	Load rates for rectangular specimens	38
30	Specimen 4 notch 1:0, notch crack opening	40

31	Specimen 4 notch 1:0, notch crack shearing and opening	40
32	Specimen 4 notch 1:0, Shear Failure	41
33	Specimen 4 notch 1:0, Flexural Failure	41
34	Specimen 2 notch 1:0 failure; side view left, top view right	42
35	Specimen 2 notch 1:0; inside centre of beam	42
36	Capacities for Rectangular Section Specimens	46
37	Time between notch initiating and ultimate failure for rectangular section specimens	47
38	Load-displacement graph for rectangular beams with notch of slope 1:0	48
39	Top and bottom strain at centre for rectangular beams with notch of slope 1:0 . .	49
40	Horizontal strain either side of notch for rectangular beams with notch of slope 1:0	50
41	Z strain location and direction	51
42	Y strain location and direction	51
43	Vertical strain either side of notch for rectangular beams with notch of slope 1:0 .	52
44	Rectangular specimen 2 notch slope 1:0; wedge defect	53
45	Horizontal strain either side of notch for rectangular beams with notch of slope 1:2	54
46	Rectangular specimen 2 notch slope 1:2; thick cut defect	55
47	Load-displacement graph for rectangular beams with notch of slope 1:4	56
48	Vertical strain either side of notch for rectangular beams with notch of slope 1:4 .	57
49	Load rates for round specimens	58
50	Specimen 2 notch 1:2, notch crack shearing and opening	61
51	Specimen 4 notch 1:4, notch crack fully opening and ultimate failure	61
52	Specimen 1 notch 1:0, existing knot at small notched section over roller support	62
53	Specimen 1 notch 1:0, final failure	62
54	Capacities for Circular Section Specimens	64
55	Time between notch crack initiation and ultimate failure	65
56	Load-displacement graph for round beams with notches of slope 1:0	66
57	Top and bottom strain at centre for round Beams with notches of slope 1:0 . . .	67
58	Horizontal strain either side of notch for round beams with notch of slope 1:0 . .	68
59	Vertical strain either side of notch for round beams with notch of slope 1:0 . . .	69
60	Top and bottom strain at centre for round beams with notches of slope 1:2 . . .	70
61	Vertical either side of notch strain for round beams with notch of slope 1:2 . . .	71

62	Vertical either side of notch strain for round beams with notch of slope 1:4	72
63	Comparison of rectangular and circular section ultimate capacities	73
64	Comparison of rectangular and circular section notch capacities	74
65	Comparison of AS1720 notch design capacities with experimental results	75
66	Comparison of Eurocode 5 notch design capacities with experimental results	76
67	Comparison of CSA O.86 notch design capacities with experimental results	77
68	AS1720 ultimate shear design capacities compared to experimental results	79
69	AS1720 ultimate bending design capacities compared to experimental results	81
70	AS1720 ultimate bending design capacities compared to experimental results	82

List of Tables

1	Wood Cell Structures	5
2	Notch Coefficient	17
3	Experimental Parameters	36
4	Properties of Spotted Gum (<i>Corymbia Maculata</i>)	37
5	Rectangular Specimen Water Contents and Initial Failure Locations	39
6	Rectangular Specimen Shear Failure Locations	43
7	Rectangular Specimen Crack Initiation and Ultimate Loads	44
8	Round Specimen Water Contents and Initial Failure Locations	59
9	Round Specimen Ultimate Failure Modes	60
10	Round Specimen Crack Initiation and Ultimate Loads	63

1 Introduction

Timber has been a dominant material in engineering and construction for centuries and continues to be a major material used in housing, floors and furniture. Timber was also the first material used to construct bridges and, although it is slowly being replaced by alternative building materials, like concrete and steel, there are currently around 20,000 timber road bridges still currently in use within Australia [1]. Many of the bridges still in use are utilised by rail which are subjected to significant load and hence the maintenance and strengthening of these bridges is of major importance [2].

Over the past few decades there has been a major decrease in the use of timber for the construction of bridges. This is predominately due to the inherent properties of timber which expose it to environmental problems such as weathering, rotting and insect infestation [1, 3]. These conditions make the bridge expensive to maintain and significantly limits the lifespan of the structure. Hence the majority of bridges now being constructed in Queensland utilise steel and concrete to minimize the impact of any environmental damage [4]. However, many timber bridges throughout Queensland still remain in use and hence require regular maintenance and strengthening to withstand growing load demands and remain stable until they are eventually replaced. As the complete replacement of bridges is expensive, the alternative of strengthening the structure appears to be the more feasible option. One of the primary sections of timber bridges which require strengthening are the notches in the timber beams. These sections are particularly prone to cracking and need to be studied in order to find a suitable method for strengthening these regions [1].

Notching is when a section from a member is cut out to ease insertion and act as seating for timber girders over piers or abutments. This is common practice in the construction of timber bridges and places increased risk of failure to the structure at the position of the notches [1]. This increased risk occurs due the section loss from notching exposing the timber to the risk of cracking and potential failure. Currently there is little information on notching design surrounding circular members or evaluating capacities of a notched round member. This is of significant importance in the construction of timber bridges as most members currently used in bridges are round. A study of the literature has revealed that there have been very few studies carried out on the behaviour of these notches in circular section beams. Hence there remains a strong need for further investigation into the behaviour of circular notched beams to develop

suitable methods of design for the construction of timber bridges.

The proposed research will provide further understanding into the effects of notches and notch angles on rectangular and round timber members. Current notch design methods will be investigated and compared to determine which method obtains the most accurate results. As many bridges are currently suffering issues caused by notching, the ability to understand the effects of notching will assist in further development of designing and possibly strengthening them. By establishing an effective method of notch design, the lifespan of current and future timber bridges may be increased and methods of maintenances can be redefined to delay the need for total replacement and overall reduce the costs associated with timber bridges.

1.1 Objectives

The aim of this research was to determine the structural behaviour of rectangular and circular section timber girders with different notched angles. The main objectives were to:

1. Determine the effects of different notch types on the flexural and shear capacity of rectangular and circular timber beams
2. Validate existing design equations for notched timber girders

1.2 Scope

The overall scope of this research was to determine the effects of notching on rectangular and circular section members, and to determine which methods of notch design yield the most accurate results. This was achieved through small-scale experiments on rectangular (60mm x 100mm x 800mm) and round (100mm diameter by 800mm length) specimens, where three different notch angles were considered; slopes 1:0, 1:2 and 1:4.

2 Literature Review

2.1 Timber Bridges

Timber has been used in the construction of bridges for thousands of years [4] and remained the preferred construction material until the middle of the 20th century when it was eventually replaced by the introduction of steel and concrete [1, 4]. Timber had remained the dominant building material because of its strength and light weight. Timber also has energy-absorbing properties, making it capable of handling short term overloads without harmful effects, making it an excellent material for bridge construction. Large timber members also have good fire resistance qualities, are relatively durable and have the ability to withstand de-icing effects. Overall the construction of timber bridges is very cost effective as timber is a relatively cheap and renewable resource and installation can usually be carried out without the need of heavy machinery, significantly reducing the labour required [4]. Although timber bridges are relatively cost effective to build, susceptibility to weather and insects make them expensive to maintain.

Ongoing repairs for the timber structure can be labour intensive and expensive, hence preventative maintenance is important in cutting costs and prolonging the life of the bridge. To prevent deterioration, the timber can be chemically treated against damage to weathering from sunlight exposure and moisture. This is a major benefit as there is little to no maintenance or painting required for wood treated with preservatives [4]. Furthermore, the wood can be treated to prevent pest infestation [1, 4] which can cause major damage to any timber structure. The commonplace use of chemical treatment to preserve timber bridges has almost certainly added decades to the life of the bridge. However, when significant damage has already occurred, strengthening may be the only feasible option to prevent further damage and eventual failure of the bridge.

The availability of suitable timber is now a major concern for existing timber bridges which require substantial maintenance throughout their structural life [1]. The ability to source large sections of wood and sawn timber is becoming increasingly more difficult as the amount of timber suitable for harvesting decreases over time. The drive for forest preservation has also increased, heavily reducing the amount of suitable timber needed for bridge construction and maintenance [1, 4]. This is another strong reason for strengthening current structures as the raw materials required for repair or replacement of timber bridges are costly and difficult to source.

2.1.1 Wood Types

There are two classes of timber; hardwood and softwood. The two types of wood can initially be distinguished by their leaves as hardwood trees have broad leaves and softwood trees have sharp needle like foliage [5].

The major difference between hardwood and softwood is their cell structures [6]. Hardwood contains mainly fibres, vessels/pores and parenchymas whereas softwoods contain tracheids (early- and latewood), resin canals and parenchymas [7].

It can be seen in Figure 1 that the cell structure of hardwood is substantially more complex than softwood [8]. The cell structure of softwood has a organised arrangement, whereas the cell arrangement of hard wood appears more random. A common misconception is that hardwood is hard in comparison to softwood, however this is not necessarily the case [9,10]. To determine whether to use softwood or hardwood, the major deciding factor is based on the intended purpose of the wood (i.e. whether it is to be in tension or compression).

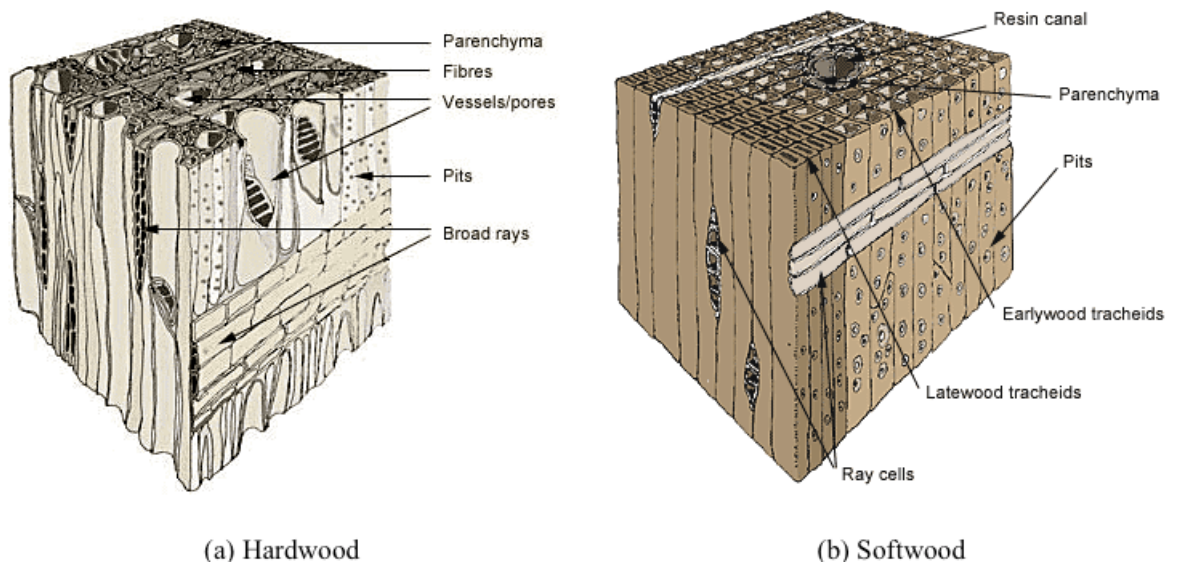


Figure 1: Wood Cell Structures [11]

Table 1 compares the aspect ratio of hardwood and softwood; these differ depending on the exact wood used and their particle/fibre size. From this it can be seen that generally hardwoods have a higher aspect ratio which implies they have better bending abilities, and thus are superior in sustaining tensile loads [12].

Table 1: Wood Cell Structures [11]

Particle size Range	Aspect Ratio	
	Hardwoods	Softwoods
20 mesh ($850\mu m - 0.85mm$)	4.6	3.5
40 mesh ($425\mu m - 0.425mm$)	4.4	3.4
60 mesh ($250\mu m - 0.25mm$)	4.4	4.2
800 mesh ($180\mu m - 0.18mm$)	4.2	4.5

More commonly used in timber bridge structures in Australia is hardwood due to its abundance at the time of construction [13], as well its combination of high strength, durability, light-weight and most importantly flexural properties [12]. Commonly used woods in Queensland bridges are spotted gum, tally-wood and swamp mahogany. Spotted gum is strong, light-weight, tough, elastic and durable, and is particularly well-performing when in tension. Tally-wood is strong, durable and very tough; it withstands underground and aqueous conditions and is used mainly in decking and posts. Swamp mahogany is elastic, strong, tough and durable, which also sustains well in underground and aqueous conditions; it is predominately used in piles [14].

2.1.2 Common Defects and Failures

There are four major defects that are commonly occurring in timber bridges; weathering, rotting, cracking and termite infestation. These defects severely reduce the lifespan of a timber bridge and will all eventually lead to member failure.

Weathering and Rotting

Weathering and rotting occur in timber members due to exposure to a combination of wind, wetting, drying and UV radiation [1, 3]. The appearance of the weathering damage depends on the elements the timber is exposed to. Exposure to high wind speeds can cause dints/abrasions from small pebbles or embedded sand particles [15], whereas exposure to a combination of running water and sun light can cause a ripple effect, as shown on a rail bridge longitudinal girder in the Figure 2.

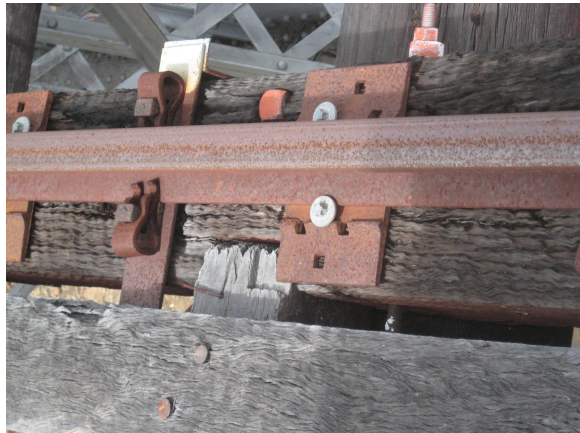


Figure 2: Weathering

Rotting occurs in areas where moisture is allowed to penetrate the wood and can lead to core rotting as shown in Figure 3 which severely reduces the strength of the member. The most vulnerable areas for rotting occur at bolt holes and cut sections (i.e. notches) where moisture can easily penetrate the timber [1, 16].



Figure 3: Core and Notch Rotting

Rot is decay caused by wood-destroying fungi which requires adequate moisture [17], heat and oxygen to prosper. This results in two different types of decay; brown rot and white rot. Brown rot is common in softwood where the fungi attacks only the cellulose creating a brown colour. However, white rot is more common in hardwood and is caused by the fungi attacking both the cellulose and lignin in the wood, creating a white colour. Rotting overall allows the rapid absorption of water and can be identified by a colour change or odor similar to anise or wintergreen [16]. Both weathering and rotting are effects of long-term exposure to the environment and can lead to a significant reduction in the strength of the member and

potentially failure.

Insects

Timber is prone to two main types of insect attack; termite and lyctids. Termites require moisture, warm temperatures, access to their nest and usually ground contact to prosper. The most effective way to avoid termite damage is to use a timber species that is resistant to termites. Alternatively, preservative treated timber can be used or a physical or chemical barrier can be created between the timber ends and the nests [3].

Only the sapwood present in specific hardwoods are vulnerable to lyctids (or powder post beetles), softwoods are resistant to attack from these insects. Thus the use of softwoods or avoidance of the used of certain susceptible hardwoods will reduce the risk on lyctid attack [3].

Both these types of insects cause the same issues in timber; where they tunnel through the wooden members, causing large amounts of intricate bored out networks. This severely reduces the member strength and can eventually cause failure [18].

Cracking

Cracking usually occurs due to applied loads (dead and live) exceeding the strength capacities of the timber member and will eventually lead to failure. This defect can occur in any conditions and is purely dependent on the loads that are applied. However the presence of other capacity reducing defects can significantly increase the chances of cracking. The two types of cracks that occur are flexural and shear cracking [1].

Flexural cracks appear on the areas of a bridge that have high moments due to applied loads. The common location for flexural cracking are at the mid-span of the member, over the support and underneath any other permanent loads (dead loads). These areas are depicted in the Figure 4 [1].

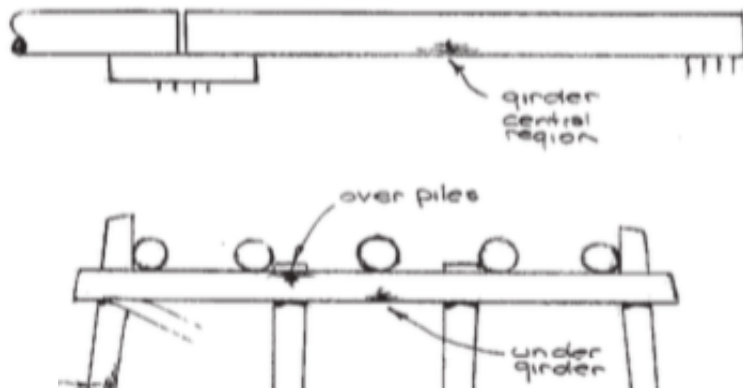


Figure 4: Locations of Flexural Cracking or Crushing [1]

Cracking due to flexure occurs in the tensile region or face of the member and can also result in the occurrence of crushing in the compression region. Hence, flexural cracking can be a combination of tensile and compressive failure [19].

Shear cracking is caused by the shear capacity of the timber being exceeded by applied loads, resulting in horizontal cracks propagating along the grain, as shown in Figure 5. These cracks occur in high shear stress regions throughout the bridge such as over piles and at the ends of girders [1].

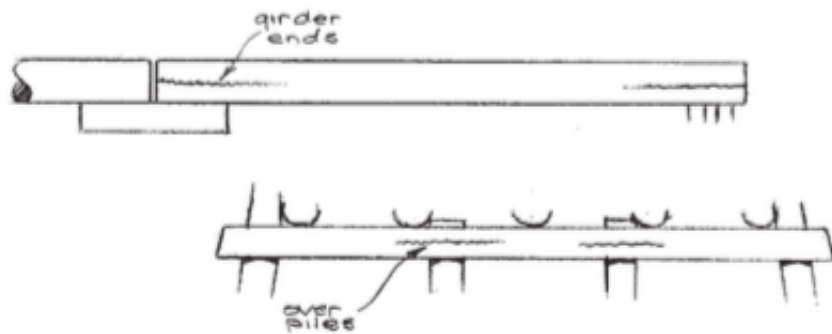


Figure 5: Locations of Shear Cracking [1]

Both flexural and shear cracking on bridges is usually a result of bending which can cause forces in tension, compression and shear as well as moments [4].

2.2 Timber Properties

Timber is a very unique structural material and differs significantly from other man-made materials, such as steel or concrete [20]. This is due to its fibrous cell structure.

The primary forms of failure in timber beams are tensile, shear and compressive failure. For timber, the stress-strain relationship is assumed to be uniaxial [21, 22], as shown in Figure 6, where the negative region describes compression and positive region is in tension.

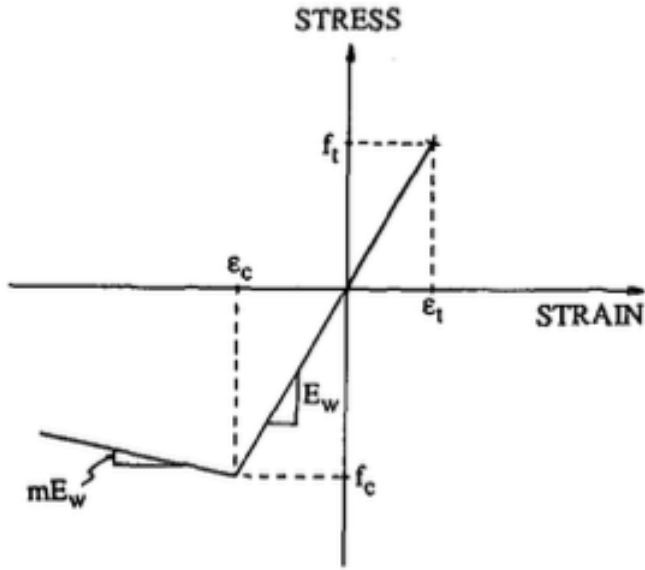


Figure 6: Standard Stress-Strain Diagram of Timber [20]

The member fails in tension at a stress f_t , with a relating strain ϵ_t , and in compression fails at a stress f_c and strain ϵ_c . The Young's modulus of the wood (E_w) is the gradient of the stress strain relationship. Beyond the compression-strain at failure (ϵ_c) the gradient and direction of the line changes by a constant ratio m of the Young's modulus [20, 23].

Tensile failure is a brittle failure and is usually caused by long-term constant distributed loading. Longer members are more susceptible to tensile failure which occurs at the weakest point on the beam. Compressive failure is also caused by long-term loading and is a ductile failure [19].

Modulus of rupture (MOR) is the maximum allowable stress a species of timber can withstand before its fibres rupture or break; which defines the bending strength [24]. It can be calculated from the maximum load the beam can carry (F_R) [25] and is given by

$$MOR = \frac{M}{Z} \quad (2.2.1)$$

$$MOR \approx \frac{3F_R l}{2bh^2} \quad (2.2.2)$$

where;

l = Span of the beam

b = Width of the beam

h = Height of the beam.

Z = Section modulus

The modulus of elasticity (MOE) measures the flexibility or stiffness of timber and is determined through bending and deflection [25, 26]. The MOE in bending, also commonly denoted as E_b , can be determined from the load at the proportional limit (F_p) [26] and is given by

$$E_b \approx \frac{F_p l^3}{4\Delta b h^3} \quad (2.2.3)$$

where;

Δ = Deflection at midspan due to the load F_p .

The flexural ability and properties is predominately due to the aspect ratio of the wood. Aspect ratio is defined as the ratio between the fibre length to the fibre thickness. Longer fibres result in superior mechanical properties compared to shorter fibres, thus a higher aspect ratio renders better flexural properties [12].

The other form of failure in wood is shear failure, which is again caused by applied shear loads exceeding the shear capacity of the beam. The shear stress distribution of a standard rectangular beam can be seen in Figure 7, and is of parabolic nature both along and perpendicular to the grain.

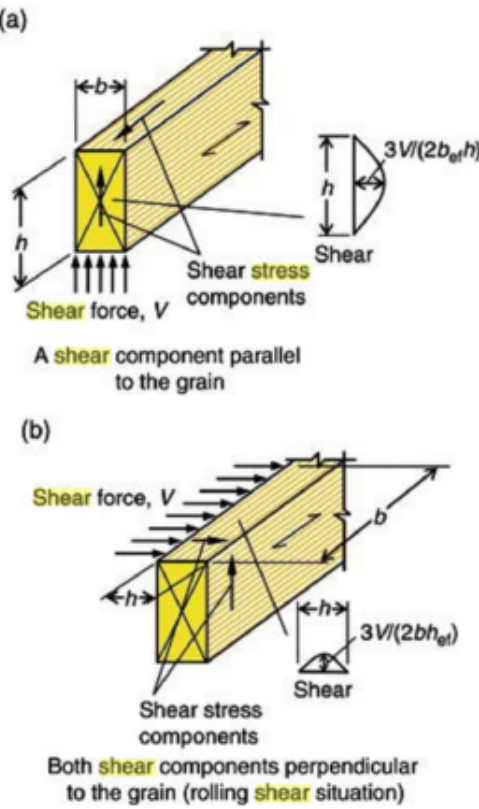


Figure 7: Shear Stress Distribution [27]

The shear capacity of a timber species is a measure of the timber fibre's ability to withstand slippage. Shear capacity in timber is much greater across the grain than along the grain, where the fibres have to be broken, than along the grain where the fibres only need to be separated from each other [25].

2.3 Australian Member Design

There are three common cross-sectional shapes of members in bridge construction; rectangular, circular and octagonal. The most commonly used is the rectangular section member, mainly for smaller scale constructions (e.g. frames, foot-bridges, etc.). However, for bridges requiring a large strength capacity, such as a rail bridge, the log can not be substantially reduced in size, as done to achieve rectangular cross-sections, thus the round and octagonal members are required.

2.3.1 Rectangular Section

There are three standard Australian design codes that discuss design processes and equation for rectangular timber members; AS1720.1, AS4676 and AS4063.

Bending

The bending capacity (M_d) for an un-notched beam, with a rectangular section, is given in AS1720.1 as

$$\phi M_d = \phi k_1 k_4 k_6 k_9 k_{12} f'_b Z \quad (2.3.1)$$

where

ϕ = Capacity Factor

k_1 = Duration of Load Factor

k_4 = Moisture Condition Factor

k_6 = Temperature Factor

k_9 = Strength Sharing Factor

k_{12} = Slenderness Factor

f'_b = Characteristic value for bending for section size

Z = Section modulus of beam about bending axis.

All factors and the strength characteristic for bending can be determined from AS1720.1.

Shear

The design capacity in shear of un-notched beams is described by AS1720.1 as

$$V_d = \phi k_1 k_4 k_6 f'_s A_s \quad (2.3.2)$$

where ϕ , k_1 , k_4 , and k_6 are as determined for bending capacity design,

f'_s = Characteristic value in shear

A_s = Shear plane area.

and the characteristic value in shear can be found in AS1720.1.

Also when the beam is loaded about its major axis in bending, the shear plane area can be

found from the breadth (b) and depth (d) using

$$A_s = \frac{2bd}{3} \quad (2.3.3)$$

2.3.2 Circular Section

The amount of information and research surrounding circular section members are minimal, and there are few design equations determined specifically for these members.

Bending

AS1720.1 uses the rectangular formula with additional factors to account for the change in section shape. This formula and additional factors are

$$\phi M_d = \phi k_1 k_4 k_6 k_9 k_{12} k_{20} k_{21} k_{22} f'_b Z \quad (2.3.4)$$

where $\phi, k_1, k_4, k_6, k_{12}$ are as for working rectangular design and

k_{20} = Immaturity Factor

k_{21} = Shaving Factor

k_{22} = Processing Factor.

Shear

The design shear capacity given by AS1720.1 is again a modification of the rectangular design approach and is given by

$$V_d = \phi k_1 k_4 k_6 k_{20} f'_s A_s \quad (2.3.5)$$

where the factors, f'_s and A_s are as specified in rectangular design, and k_{20} takes into account the maturity of the material. The shear plane area for a round member is

$$A_s = \frac{3\pi d^2}{16} \quad (2.3.6)$$

2.3.3 Octagonal Section

Queensland Department of Transport and Main Roads (TMR) suggests that the design of such members for bending, is the same as for rectangular sections [1]. However there is very little information surrounding octagonal member design and no design methods determined specifically for this cross-section.

2.4 Notching

Notching or sniping is when the lower corner of a member is cut to make insertion easier, and to increase the stability of the member when sitting on a pier/abutment. One of the major issues faced with notches are they significantly reduce the load-carrying and shear capacities of timber beams. For these reasons, it is suggested that the use of notches be avoided in practice, however in some situations they cannot be [28, 29].

The reduction in the shear capacity of the beam causes a brittle failure and cracking to initiate from the corner of the notch, and propagate along the direction of the grain [1, 28]. Figure 8 indicates the common behaviour of notch cracking.

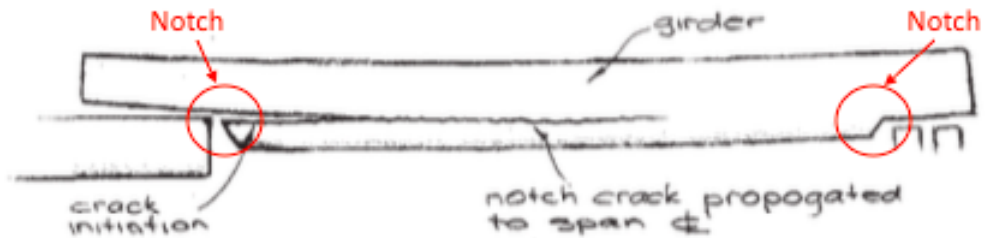


Figure 8: Notch Cracking [1]

To reduce the effects of capacity loss, TMR limit the section area loss from notching to be a maximum of 10%. In cases where the notch is strengthened, a maximum allowable section loss can be up to 25% [1]. As shown in Figure 9, TMR also specifies that if there is less than 75% of the original depth over the support, there is a high chance of failure to occur in bending.

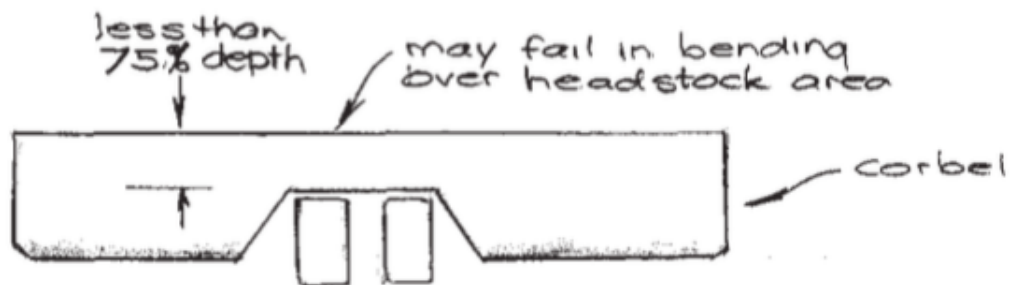


Figure 9: Member failure in bending over support [1]

There are three different types of fracture modes of a notch in a timber member which are dictated by the forces/stresses present at the notch corner. Figure 10 depicts these modes.

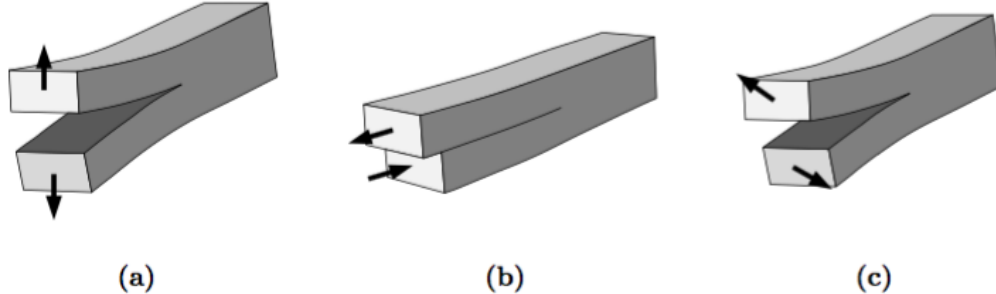


Figure 10: Fracture Modes (a) mode 1 (b) mode 2 (c) mode 3 [29]

Fracture mode 1 is when the crack propagating from the notch opens and is caused by tensile forces at the notch corner. Mode 2 is horizontal cracking/shearing, cause by shear forces acting along the grain at the notch corner. Lastly, mode 3 is a mixed mode fracture and is caused by a combination of both tension and shear forces [29].

2.4.1 Notch Types

There are four main types of notching, rectangular end notch, tapered end notch, rounded end notch and notch in span. The figure below shows the geometry of each type of notch.

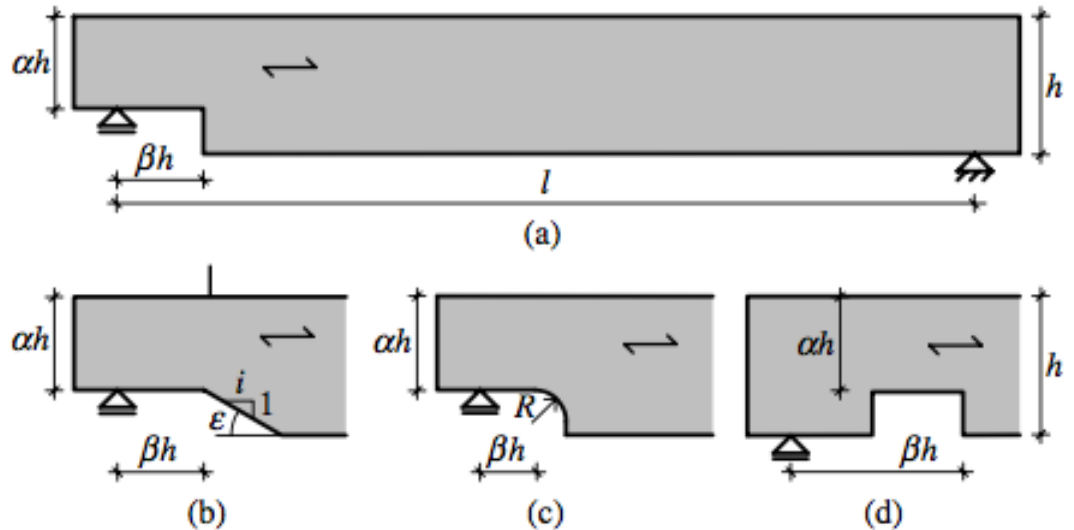


Figure 11: Notching Types; (a) rectangular end notch; (b) tapered end notch; (c) rounded end notch; (d) notch in span [28]

There is little information surrounding the exact effects of each type of notch on members. However, it is recommended by Australian Standard AS1720.1 that a tapered notch with a 1:4 gradient chamfer from the notch corner be used if notching is required. In theory, this particular tapered notch will increase the member's shear capacity by three times in comparison to a rectangular end notch [1].

2.4.2 Notch Design

There are many different methods for designing notched members, based on significantly different concepts and, in most cases, obtaining varied results [29]. There are few methods in designing round end notches and notches within member spans, and most standards only design for a rectangular or tapered notch. However, the greatest limitation in notch design is all methods are based on rectangular section beams and do not account for circular or octagonal sections [1]. This is a major issue, as round and octagonal sections are preferred in timber bridges, due to their larger sections.

Australian Standards

The notched member design method used in AS1720.1 focuses on stress intensities and accounts for the effects of the maximum bending moment (M^*) and maximum shear force (V^*) occurring at the corner of the notch; where any negative values for bending moment or shear are neglected [29]. AS1720.1 notch design equation is

$$\frac{6M^*}{bd_n^2} + \frac{6V^*}{bd_n} \leq \phi g_{40} k_1 k_4 k_6 k_{12} f'_{sj} \quad (2.4.1)$$

where

f'_{sj} = Shear strength

g_{40} = Notch coefficient.

The k-factors and ϕ are purely dependent on location, use and specific timber characteristics, and are found as per usual design methods in AS1720.1. The other variables used in equation 2.4.1 are depicted in Figure 12.

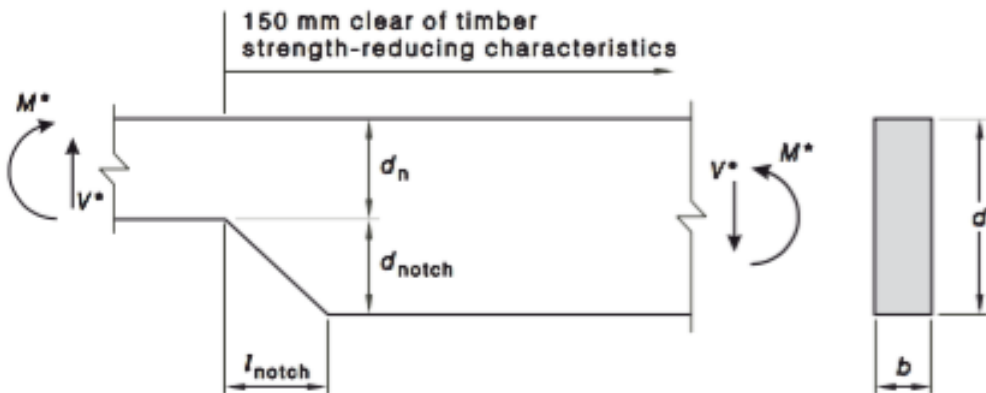


Figure 12: Notation for Notch

The notch coefficient g_{40} depends on the taper and height of the notch and can be found according to Table 2.

Table 2: Notch Coefficient

Notch Angle Slope	g_{40}	
	$d_{notch} \geq 0.1d$	$d_{notch} < 0.1d$
$l_{notch}/d_{notch} = 0$	$9.0/d^{0.45}$	$3.2/d_{notch}^{0.45}$
$l_{notch}/d_{notch} = 2$	$9.0/d^{0.33}$	$4.2/d_{notch}^{0.33}$
$l_{notch}/d_{notch} = 4$	$9.0/d^{0.24}$	$5.2/d_{notch}^{0.24}$

AS1720.1 specifies that for this design method, no strength-reducing characteristics, such as knots, are allowed within 150mm from the notch corner.

Australian design method is based on linear elastic fracture mechanics (LEFM), which is basic fracture mechanic concepts under the assumptions that the material is linearly elastic. However this assumption is not ideal for timber, as it's elastic properties are considered orthotropic.

Fracture Mechanics

The AS1720.1 notched member design method considers only the effect of stress intensities and does not take into account fracture mechanics. In 1988, Gustafsson proposed an equation to design for strength of the notch, based on fracture energy [28, 30].

$$\frac{V_f}{bod} = \frac{\sqrt{\frac{G_c}{d}}}{\sqrt{0.6 \frac{(\alpha - \alpha^2)}{G_{xy}}} + \beta \sqrt{6 \frac{(1/\alpha - \alpha^2)}{E_x}}} \quad (2.4.2)$$

Where;

V_f - Shear force at fracture of notch

G_{xy} - Shear modulus

E_x - Modulus of elasticity in beam direction, parallel to the grain

d - depth of the member

G_c - Fracture energy

β , α and h are depicted in the figure below.

This equation was established for a beam notched at both ends, and in accordance with the characteristics shown in the figure 13. The actions due to the moment and shear, along with the effect from elastic clamping, results in a deflection, which is the basis of this fracture energy approach. Gustafsson derived this deflection, also considering lower bending stiffness of the cross-section at the junction of the notched part of the beam, and assumed its proportionality to the moment acting at the notch corner [28]. Clamping was also incorporated with a factor, which was conservatively chosen as $1/\alpha^3$ [30].

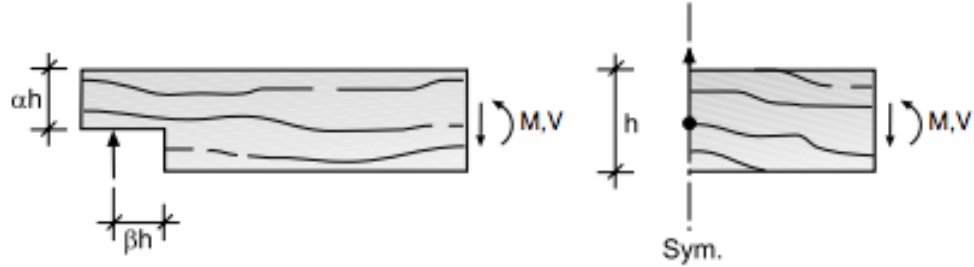


Figure 13: Geometry of notched beam and dowel joint [31]

The fracture energy for a notched member can be found using the following equation [31].

$$G_c = \frac{1}{2} (P_f^2 / B) \frac{dC(a)}{da} \quad (2.4.3)$$

Where;

C - denotes the compliance of the structure

da - extension of the length of the crack

P_f - magnitude of load that start propagation of the crack

B - width of the fracture area (i.e. $B = dA/da$)

Similar notch strength equations have been derived (Smith et al. 1996), with a defining difference of the clamping effect. Smith et al proposed a notch strength relationship from the

same fracture mechanic concepts, but taking a clamping factor of $1/\alpha^2$. It has been found through comparison, that the prediction of the notch strength proposed by Gustafsson was more conservative and accurate than Smith et al. which has given results exceeding the notches capacity [28].

This approach is used as a verification of the shear stress in the notch cross-section and has become a basis for design methods in European and Canadian design codes.

Eurocode 5 Approach

The European timber structure design code (Eurocode 5) is based on studies of notch fracture mechanics and specifies the following equation for notch design as

$$\tau_d = 1.5 \frac{V}{bh_{ef}} \leq k_v f_{v,d} \quad (2.4.4)$$

where

τ_d = Shear stress

V = Shear force

h_{ef} = Depth above notch

The shear strength, $f_{v,d}$, can be found using

$$f_{v,d} = \frac{k_{mod} f_{v,k}}{\gamma M} \quad (2.4.5)$$

where $f_{v,k}$ is the characteristic shear strength, k_{mod} is a strength modification factor and γM is a material modification factor, all of which can be found in Eurocode 5 [32].

The notch factor k_v is derived from Gustafsson's 1988 equation [30], as well as modifications to account for the taper of the notch (i) established by Riberholt [33] and is given by

$$k_v = \min \left\{ 1, \frac{k_n(1 + \frac{1.1i^{1.5}}{\sqrt{h}})}{\sqrt{h}(\sqrt{\alpha(1-\alpha)} + 0.8\frac{x}{h}(\sqrt{\frac{1}{\alpha}} - \alpha^2))} \right\} \quad (2.4.6)$$

Overall, the notch factor considers the notch taper i , material constant k_n , ratio of depth above

notch to total depth α , the distance to the support x , and the total depth of the beam h [1, 29].

CSA O.86 Approach

The Canadian design code (CSA 0.86:2014) is also based on fracture mechanics and thus has a similar design concept to Eurocode 5 [29]. However, the design is based around the verification of the resistance of the notch (F_r) instead of the stresses, which is calculated by

$$F_r = \Phi F_f A K_N \quad (2.4.7)$$

where

Φ = Resistance factor (given as 0.9)

A = Cross-sectional area

F_f can be calculated from f_f and Equation 2.4.8 [34, 35].

$$F_f = f_f K_D K_H K_{S_{tp}} K_T \quad (2.4.8)$$

Where f_f is given as 0.5MPa for sawn lumber and the condition (K) values can be found in CSA O.86.

K_N is the notch factor and can be found using Equation 2.4.9 [29, 34]. The notch factor is based on studies by Smith and Springer, and takes into account the depth of the beam (d), notch ratio α and notch length ratio η [36].

$$K_N = \left\{ 0.006d \left[1.6 \left(\frac{1}{\alpha} - 1 \right) + \eta^2 \left(\frac{1}{\alpha^3} - 1 \right) \right] \right\}^{-1/2} \quad (2.4.9)$$

where

d = Total depth of member

d_n = Depth of notch

e = Length to notch from centre of support

$\alpha = 1 - d_n/d$

$\eta = e/d$

To satisfy CSA O.86 design requirements, the design shear load (Q_f) must be less than the notch resistance load (F_r) [34, 35]. This method only considers the effects of a rectangular end notch (slope 1:0), and does not account for different notch angles.

2.5 Timber Strengthening

There are many methods used to strengthen timber structures [20]. These techniques are based around combining various different forms of reinforcement to the members. Basic forms of reinforcement have been utilised such as steel bars, steel and aluminium plates and externally bonded plywood. There have also been some slightly more complex strengthening efforts. In 1965, Peterson [37] attempted to prestress glulam timber beams using stressed steel plates. This was achieved by fixing the steel plates to the tension side of the glulam beam using epoxy. Others include pre-stressing glulam using cable and strengthening using steel tension bearing embedded wire.

A popular form of reinforcement of timber beams is the use of fibre reinforced polymers (FRP) composites. This form of reinforcement is unique because of its ability to improve structural strength, stiffness and ductility characteristics, maintaining a very light weight [20]. Although many methods of timber strengthening has been tested, there are few recorded efforts in testing strengthened notched timber members.

2.5.1 Strengthening of Notched Beams

Due to the abrupt change in the section area from a notch, high stresses are concentrated at the corner of the notch and can develop cracks. Extensions of these cracks can lead to failure and thus reinforcing notches is required to reduce the risk of cracking [29]. Notches can be reinforced either internally (Figure 14) or externally (Figure 16). Internal reinforcements are usually screwed/glued in rods and fully threaded screws. It should be noted that the screws and rods must be tight fitting to reduce the impact of shrinkage and water penetrating the hole [29, 38].

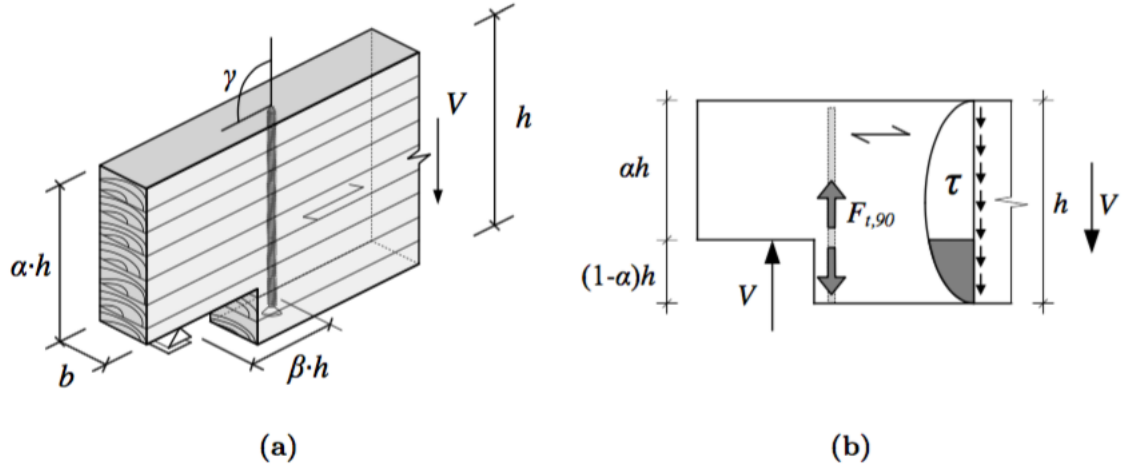


Figure 14: (a) Parameters of internal reinforcement (b) The theoretical portion of the shear stress taken by the reinforcement [29]

Bolts have been used as a standard notch strengthening method by TMR and are commonly M24 galvanised bolts, inserted perpendicular to the grain and extending through the full depth of the member. A 3mm thick plate is used at either end of the bolt to reduce cracking and pull out effects. The bolts are threaded at both ends and held on by nuts as shown in Figure 15 [1]

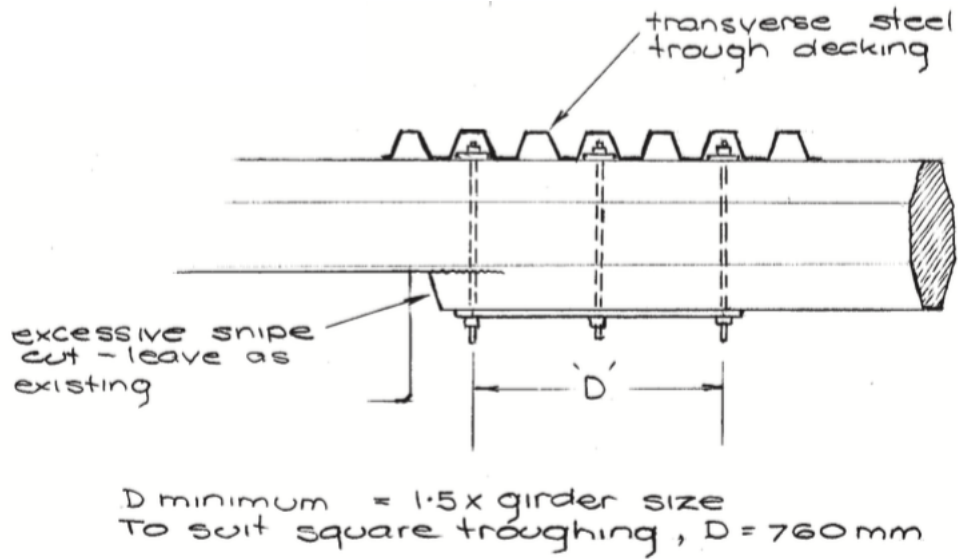


Figure 15: TMR Standard Bolt Layout [1]

External notch reinforcement methods are commonly adhered plywood, LVL or lamellas of solid timber and metal plate fasteners [29,38]. These are used to increase the strength capacities of the notch corner and reduce the risk of cracking.

Steel straps have also been used by TMR to reduce notching effects on piles, as seen in Figure 16. However this method has not been used to reinforce girders. Essentially, a strap works

similarly to a plate or wrap, where it compacts the notch corner and reduces the effects from notch cracking.

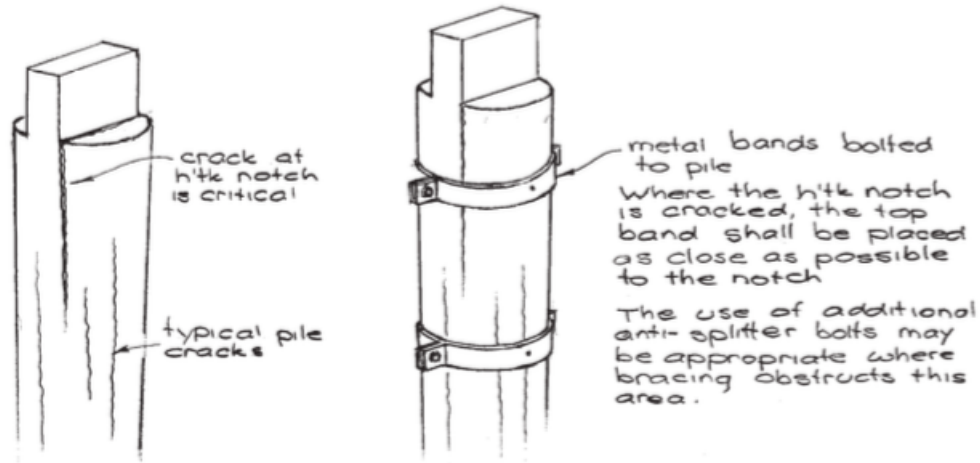


Figure 16: Straps on Piles [1]

Studies have been undertaken comparing reinforcement methods, however were only carried out on rectangular sectioned beams, and no other sections have been considered [29].

2.6 Analysis and Modelling

For analysis and modelling purposes, timber can be assumed to have orthotropic properties in the longitudinal, tangential and radial directions [39]. These directions are shown in Figure 17 with relation to the cross-sectional grain direction, where L refers to longitudinal, R to radial and T tangential. This will assist in developing accurate models using finite element analysis (FEA) of a three-dimensional member.

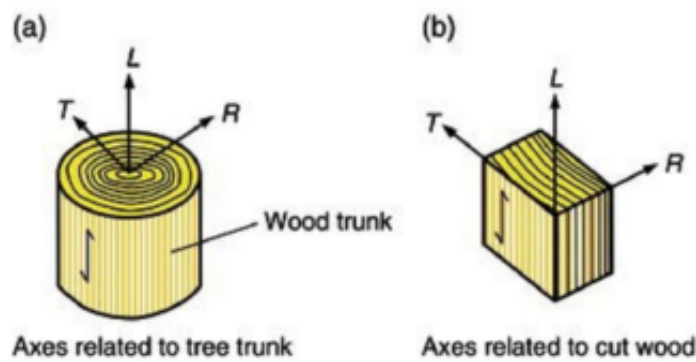


Figure 17: Wood Axes [27]

Finite element analysis has been used throughout previous notched timber beam studies to determine the theoretical behaviour of the notch with different slope angles and lengths [29].

Research of notching through means of FEA by Jockwer, in 2014, determined that the energy release rate at the notch corner decreased with an increasing notch slope. The energy release rate dictates the crack growth and overall a higher energy rate implies a faster crack growth, which will likely occur sooner than a lower energy rate [29].

3 Materials and Methodology

Notches are widely used throughout timber bridge construction as a method of seating over other members or piers. Due to the section loss caused by notching, horizontal splitting commonly occurs along the grain, which may result in failure. This is caused by high stresses occurring in the notch corners, particularly in shear, combined with a loss of member capacity due to the reduced area. Although there are design methods for notching, they differ between codes and are based on rectangular sections. This is a major issue as members commonly used in timber bridges are of circular section. To achieve a better understanding of notch behaviour and current design methods, the following experiments and numerical testing were undertaken.

1. Small scale tests on rectangular and round members were carried out to determine the critical notch angle for each profile and its effects on the shear/bending capacity of the timber beam

3.1 Preliminary Results

3.1.1 Finite Element Analysis

A FEM model of the rectangular 1:0 slope notch specimen was completed on ANSYS V16.0 for the experimental specimen, to establish the optimum placement for data reading equipment and critical loading set-out for all tests. The model was drawn to replicate the exact specimen intended and set-up to be used for testing, with a width of 60mm, depth of 100mm and 800mm length. The specimen also had a 30mm deep notch on one side, which was notched in 200mm, and the simple supports sat 100mm in from either end. To evaluate the model, specific properties were used for ANSYS and can be seen in Figure 18.

	A	B	C	D	E
1	Property	Value	Unit	<input checked="" type="checkbox"/>	<input type="checkbox"/>
2	Density	1060	kg m ⁻³	<input type="checkbox"/>	<input type="checkbox"/>
3	Orthotropic Elasticity			<input type="checkbox"/>	<input type="checkbox"/>
4	Young's Modulus X direction	2400	MPa	<input type="checkbox"/>	<input type="checkbox"/>
5	Young's Modulus Y direction	1500	MPa	<input type="checkbox"/>	<input type="checkbox"/>
6	Young's Modulus Z direction	26000	MPa	<input type="checkbox"/>	<input type="checkbox"/>
7	Poisson's Ratio XY	0.66		<input type="checkbox"/>	<input type="checkbox"/>
8	Poisson's Ratio YZ	0.047		<input type="checkbox"/>	<input type="checkbox"/>
9	Poisson's Ratio XZ	0.045		<input type="checkbox"/>	<input type="checkbox"/>
10	Shear Modulus XY	579	MPa	<input type="checkbox"/>	<input type="checkbox"/>
11	Shear Modulus YZ	1338	MPa	<input type="checkbox"/>	<input type="checkbox"/>
12	Shear Modulus XZ	2000	MPa	<input type="checkbox"/>	<input type="checkbox"/>

Figure 18: Properties used for ANSYS simulation

Figures 19 to 21 show the ANSYS analysis for the rectangular end notched specimen, centrally loaded and simply supported. The location of the load was chosen as the model suggested that this location for loading would give the most critical effects and reduce any failure due to crushing over the notch. The loading location was chosen through trial and error in the ANSYS model.

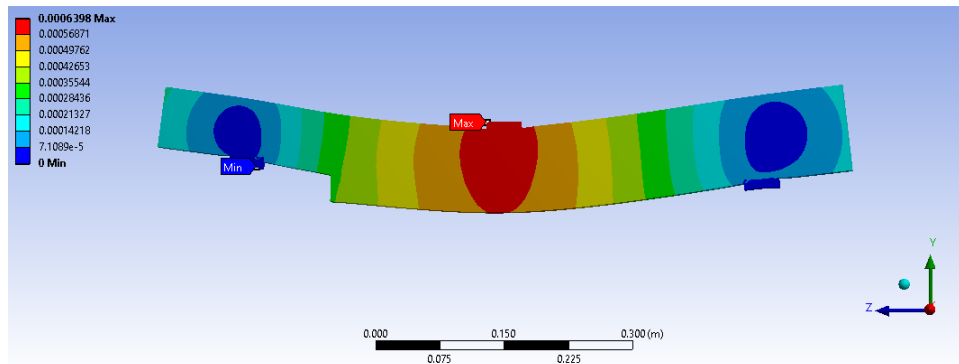


Figure 19: Rectangular Section Beam: deflection

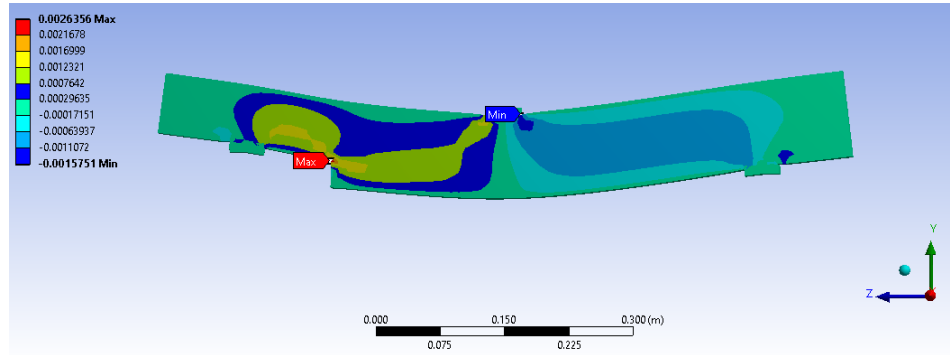


Figure 20: Rectangular Section Beam: XY-plane shear strain

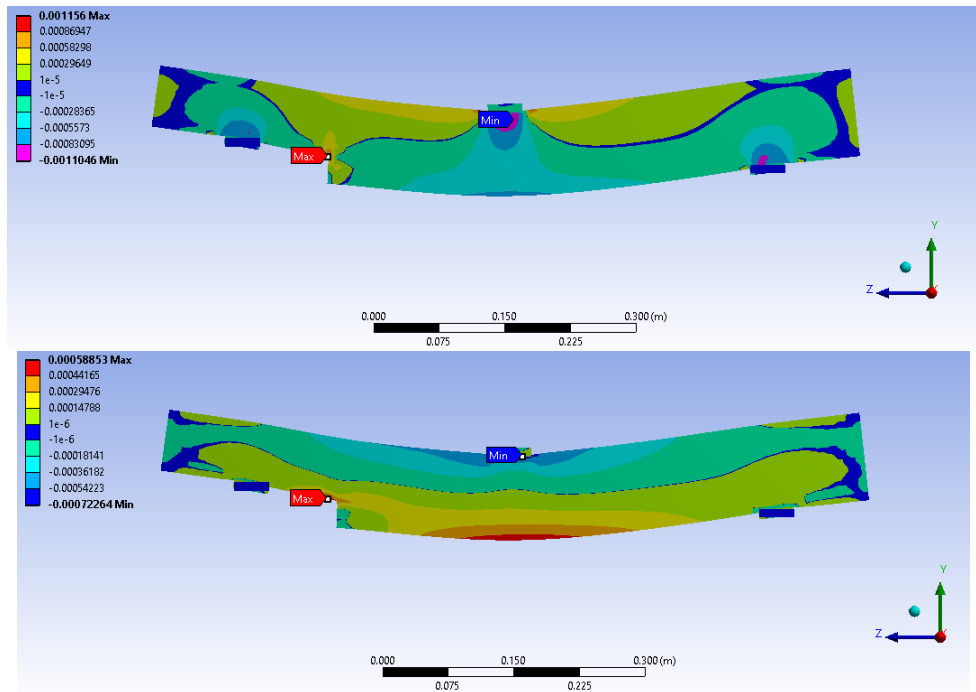


Figure 21: Rectangular Section Beam: normal strain in Y-direction (top) and Z-direction (bottom)

From Figures 19 to 21, it was observed that the strains were most critical within a 5mm radius around the notch corner with the deflection being most critical at the centre of the beam. Figure 21 also indicated a large amount of compressive strain would occur directly beneath the loading plate, and tensile strain on the bottom face, in line with the load. These results ultimately defined the placement of the strain gauges and LVDT.

3.2 Experimental Set-up

A three point loading set-up was used for all member testing throughout the experiments. The set up consisted of a centrally loaded, simply supported beam. Steel plates with dimensions

5mm x 40mm x 60mm were used over the supports to distribute the load onto to beam. All timber used were of the same species and dimensions. The tests were carried out for both rectangular and circular section members and the moment of inertia and section modulus for both types of beams were assumed to approximately constant. This will allow comparison in design methods and results. A Linear Variable Differential Transformer (LVDT) was also used to measure the deflection at the centre of the beam, as well as a 600kN capacity load cell, which was used to measure the applied load. To collect all the data from the strain gauges, LVDT and load cell, a CR3000 Campbell's scientific data logger was used.

The rectangular members tested were 60mm wide x 100mm deep x 800mm long, back sawn timber. Allowing for the 30% maximum depth loss, the notches were cut to a depth of 30mm, and were cut so that the notch corner sat 200mm in from the end of the specimen. The specimens were notched at one end only, to ensure any notch failure would be concentrated at that notched end only. This allowed us to decrease the number of strain gauges required to record data. The test set-up for the rectangular experiments can be seen in Figure 22.

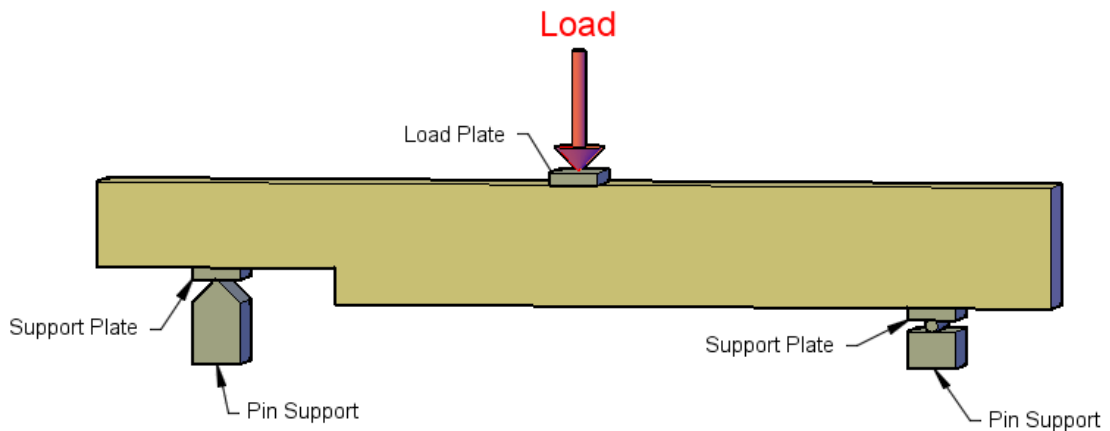


Figure 22: Rectangular Member Test Set-Up

The supports were 600mm apart, from centre to centre, and the member was placed so it sat over the support at 100mm in from either end (100mm from notch corner). A 5mm x 40mm x 60mm steel plate was also placed at the centre of the beam and under the point load to distribute the load. The tests were set-up within a 1000 kN capacity Avery MTS machine, where the MTS applied a load at a constant rate. AS1720 specifies instantaneous load rating to be a rate at which the member fails within a time frame of 5mins. After some alteration, the load rate was set to 10kN applied load per minute to comply with AS1720.

The round members used were 800mm in length with a 100mm diameter, which was design

to maintain a similar moment of inertia with the rectangular member. The notch was cut to a depth of 25mm, which was chosen to stay within Department of Transport and Main Road's maximum limitations of 25% depth loss. These members were sawn so their grain profile was radial.

The same set-up was used for the round specimens as used for the rectangular; with a simply supported, 3 point load set up, 600mm effective length between supports, and the specimen supported 100mm in from either end. The same MTS machine was used at the same loading rate applied, for ease of later comparison with the rectangular specimen results. This set-up can be seen in Figure 23.

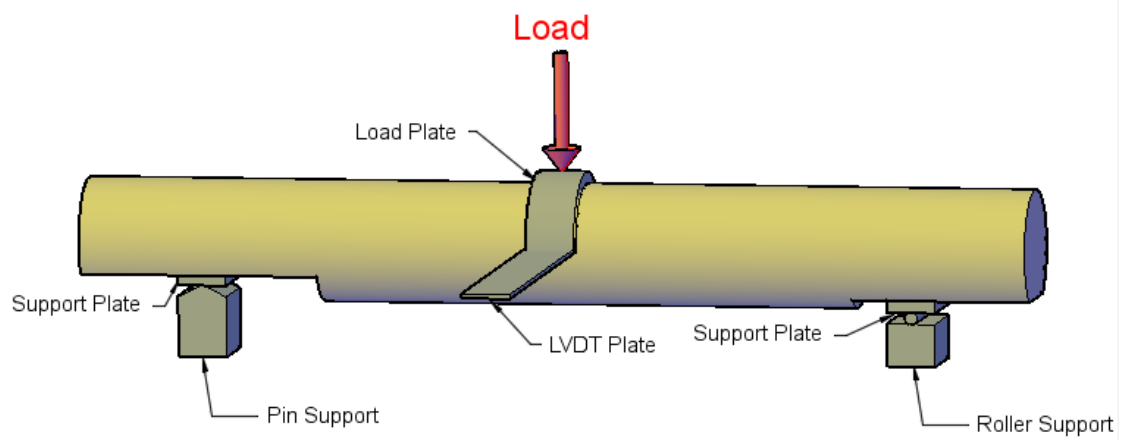


Figure 23: Round Member Test Set-Up

A rounded 5mm thick by 40mm wide metal loading plate was made, curving half of the members circumference, with a 3mm x 40mm x 300mm long, straight piece of metal welded to one side to support the LVDT. This plate can be seen in Figure 24.



Figure 24: Loading and LVDT Plate for Round Specimen

Specimen Documentation

Before any testing was undertaken, the specimens were required to be documented in great detail, to account for any inaccuracies or defect interference with experimental results. Firstly, the length, width, depth, average diameter, notch length, notch depth and mass were measured and recorded. The specimen was then carefully checked for defects and imperfections (i.e. knots, rot, cracks etc.). These were measured, photographed and documented and the process was repeated for all 24 specimens.

Specimen Strain Gauge Implementation

The locations for the expected maximum loading effects on the beam were determined using ANSYS modelling and strain gauges were placed in these locations for all specimens tested. As shown in Figure 25, a 2mm (FLA2-11-3L) strain gauge were vertically placed 5mm from the notch corner. A 30mm (PFL-30-11-3L) strain gauge was placed horizontally, directly next to the vertical strain gauge. This arrangement was mirrored on both sides of the notch, and a 30mm strain gauge was placed centrally on the top and bottom of the centre of the beam. These strains were used to determine an overall stress profile for the notch and the centre of the beam. This would provide valuable information on the reaction of the notches due to the applied loads

The strain gauges were then attached to the specimen using the corresponding strain gauge adhesive. The 30mm strain gauges were centrally placed at the top and bottom of the beam, running along the grain. This process was repeated for all specimens.

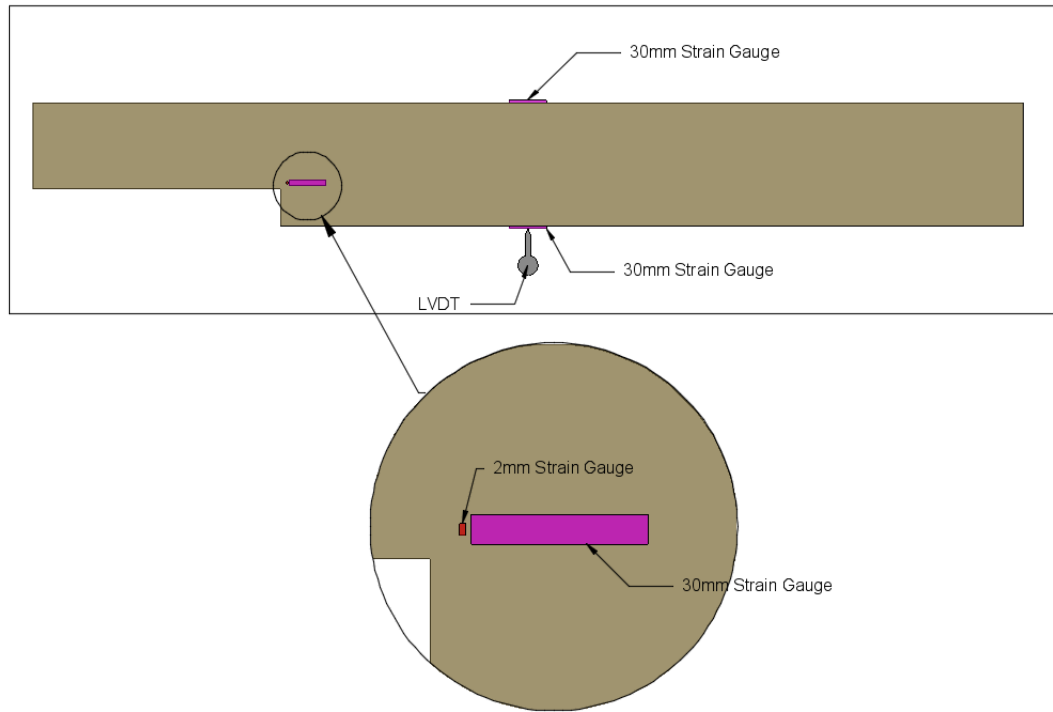


Figure 25: Strain Gauge and LVDT Layout

LVDT Implementation

For the rectangular specimens, piece of plywood (20cm x 20cm x 5cm) was attached to the specimen and mid-span using super glue. Once it was dry and secured, a 50mm LDVT was magnetically attached to the MTS machine and placed directly above the piece of plywood. For the round specimens, a long metal plate was incorporated into the constructed curved loading plate, which extruded horizontally from the centre of the beam to allow seating for the LVDT.

Camera Implementation

A 400fps camera was used to video the notch of each specimen during loading. The camera was connected to a magnetic lever arm which would magnetically attach to the MTS machine. This allowed the camera to be moved to the optimal position to capture the notch failure for each experiment.

Timber Specimen Test Set-Up

Once the strain gauges had been securely attached, the specimen was prepared to undertake loading. To set-up the experiment, the timber specimen was placed upon the simply supported arrangement within the MTS machine. This arrangement consisted of the notched end supported by a pin support and un-notched end supported by a roller, as shown in Figure 26. The

metal support plates were then slipped under the member to sit centrally above the two end supports, with extreme care taken to not interfere with any strain gauges throughout the set-up.

Data Logger Set Up

After the specimen experimental arrangement was complete, the strain gauges, LVDT and Load Cell were connected to the data logger. This was achieved by wiring 8 ports of the data logger with long wires that had alligator clips at the opposing ends.

Timber Specimen Testing

Once the specimen was correctly placed, set-up and all strain gauges and the LVDT was connected, the load cell was placed on top of the loading plate, a steel disc and a steel ball. A 5mm x 100mm x 100mm steel loading plate was then placed on top of the load cell, and the MTS load was lowered until it was just touching the top loading plate. Before we began loading, the data logger readings from the strain gauges, LVDT and load cell were checked to determine if all were properly connected and collecting data, the overall set-up can be seen in Figure 26.



Figure 26: Set-up of loading plates, metal ball and load cell in MTS Machine

Finally, the data logger was zeroed, and the MTS machine applied a load at a constant rate until the specimen reached ultimate failure. This set-up and testing process was the same for all 24 specimen, and all experiments were completed in the James Cook University structural engineering lab. All data from the strain gauges, LVDT and load cell was then analysed in conjunction with video footage of the experiment to align points of cracking and failure.

Specimen Moisture Content

Immediately after each specimen was tested, and had failed, the water content was taken, using a moisture meter. The water content was taken from three different points inside the beam, which was cracked open, and then averaged. This was repeated for every specimen, except for the first three rectangular 1:0 slope specimens, as the moisture meter was not available during their testing.

3.2.1 Altering Notch Angles of Small Scale Members

Three notch slopes were tested in this experiment; slopes 1:0, 1:2 and 1:4. These notch slopes were chosen as they are commonly used in timber bridging and have direct design methods in AS1720, which can be used for later comparison. The strains surrounding the notch and failure type were observed to determine the critical notch angle.

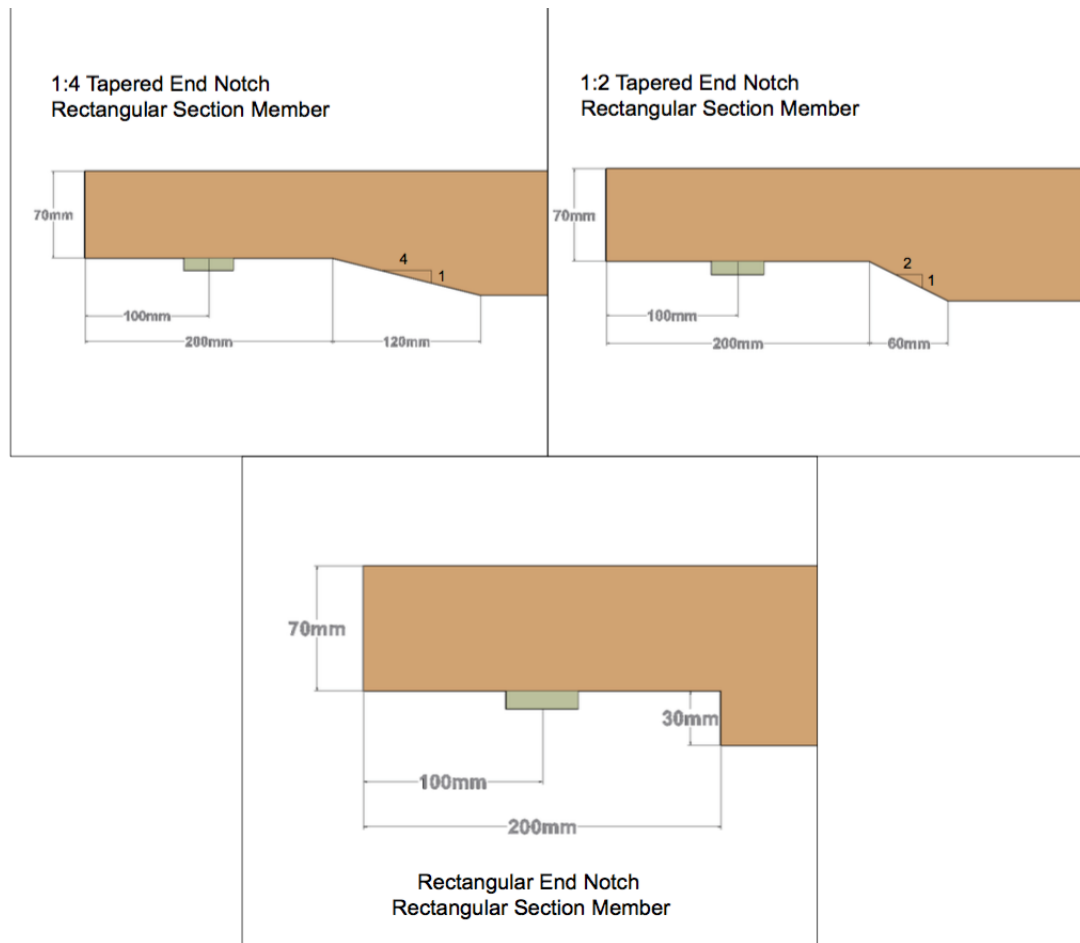


Figure 27: Notch Profiles for Rectangular Section Members

A set of 4 specimens were tested for each notch angle in both rectangular and circular section. The notch layout for each test can be seen in Figures 27 and 28.

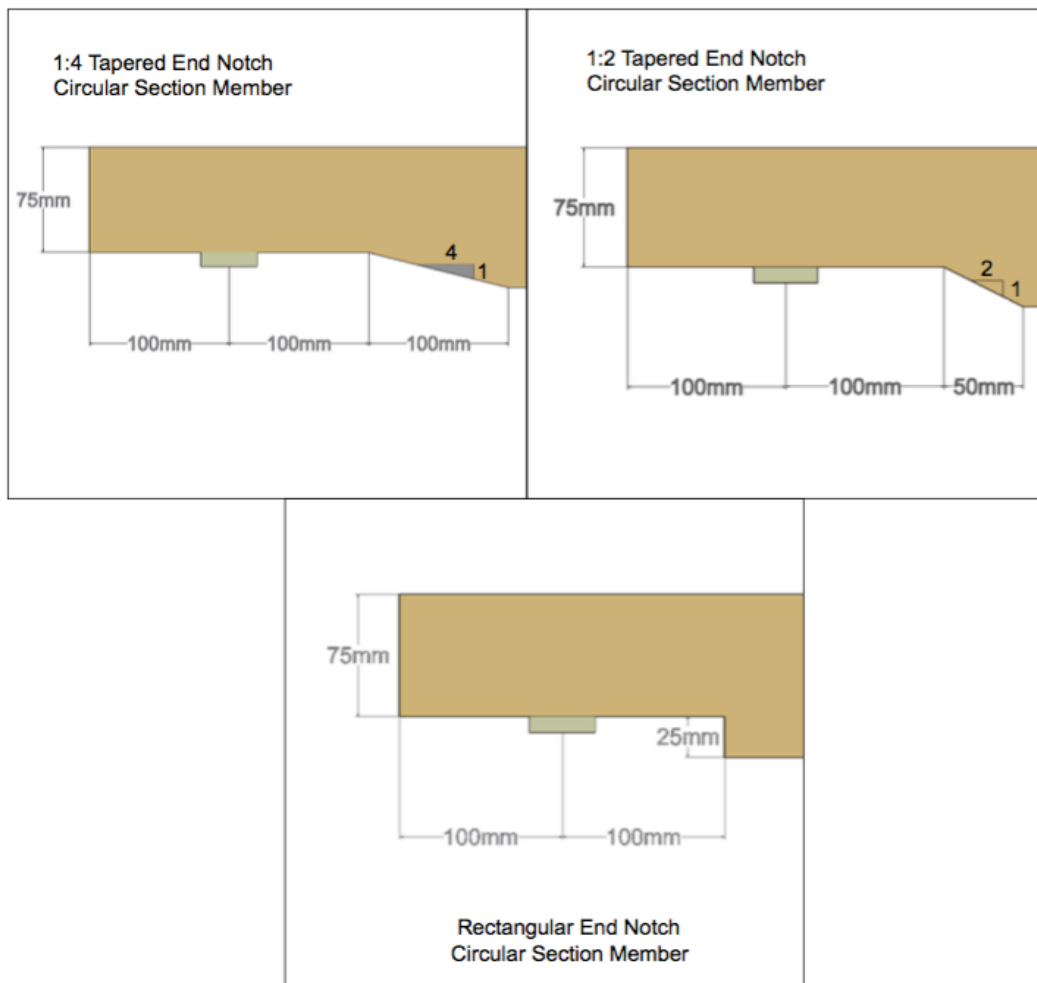


Figure 28: Notch Profiles for Circular Section Members

Table 3 shows the set experimental parameters for each section shape and notch profile. As it can be seen, the moment of inertia between the two section is approximately equal.

Table 3: Experimental Parameters

Rectangular Section							
Notch Profile	Notch Angle Slope	Member Depth (mm)	Width (mm)	Notch Depth (mm)	Total Section Area (mm^2)	Area Above Notch Corner (mm^2)	Moment of Inertia ($10^3 mm^4$)
1	1:0	100	60	30	6000	4200	5000
2	1:2	100	60	30	6000	4200	5000
3	1:4	100	60	30	6000	4200	5000
Circular Section							
Notch Profile	Notch Angle Slope	Diameter (mm)		Notch Depth (mm)	Total Section Area (mm^2)	Area Over Notch Corner (mm^2)	Moment of Inertia ($10^3 mm^4$)
1	1:0	100		25	7850	6320	4910
2	1:2	100		25	7850	6320	4910
3	1:4	100		25	7850	6320	4910

3.3 Material Properties

Timber Properties

The timber used for testing was spotted gum (*corymbia maculata*) timber, as it a hardwood that is commonly used in Queensland bridges currently being utilised. The properties and characteristics of spotted gum timber are given in Table 4 [40, 41]. All specimens were unseasoned and green (have a water content greater than 12%) and were sourced from Grays Sawmill in Proserpine, Queensland. It should also be noted that the strength grades of this timber were determined through a combination of previous studies, literature and standard codes [40, 41].

Table 4: Properties of Spotted Gum (*Corymbia Maculata*) [40, 41]

Properties		Moisture Content 12%	Green (MC > 12%)	Dry (MC < 12%)
Modulus of Rupture MOR (MPa)	<i>Longitudinal</i>	141.1	99	150
	<i>Radial</i>	19.5		
	<i>Tangential</i>	14.9		
Modulus of Elasticity MOE (MPa)	<i>Longitudinal</i>	26174	18000	23000
	<i>Radial</i>	2405	1531	
	<i>Tangential</i>	1499	665	
Shear Modulus G (MPa)	<i>Long - Rad</i>	1736		
	<i>Rad - Tang</i>	840		
	<i>Long - Tang</i>	1530		
Poisson's Ratio ν	<i>Long - Rad</i>	0.49		
	<i>Long - Tang</i>	0.550		
	<i>Rad - Tang</i>	0.660		
	<i>Rad - Long</i>	0.045		
	<i>Tang - Rad</i>	0.480		
	<i>Tang - Long</i>	0.047		
Bending Strength (MPa)		142		
Compressive Strength (MPa)		76		
Tensile Strength (MPa)		159		
Density (kg/m^3)		1060	1150	1100
Strength Group (AS1720)			S2	SD2
F-Grade (AS1720)			F14	F22

4 Results and Discussion

4.1 Rectangular Specimens

4.1.1 Loading Rates

The loading rates used to load the rectangular specimens can be seen in Figure 29. It can be seen that the load rate was constant throughout loading all specimens, at a load rate of 10kN per minute.

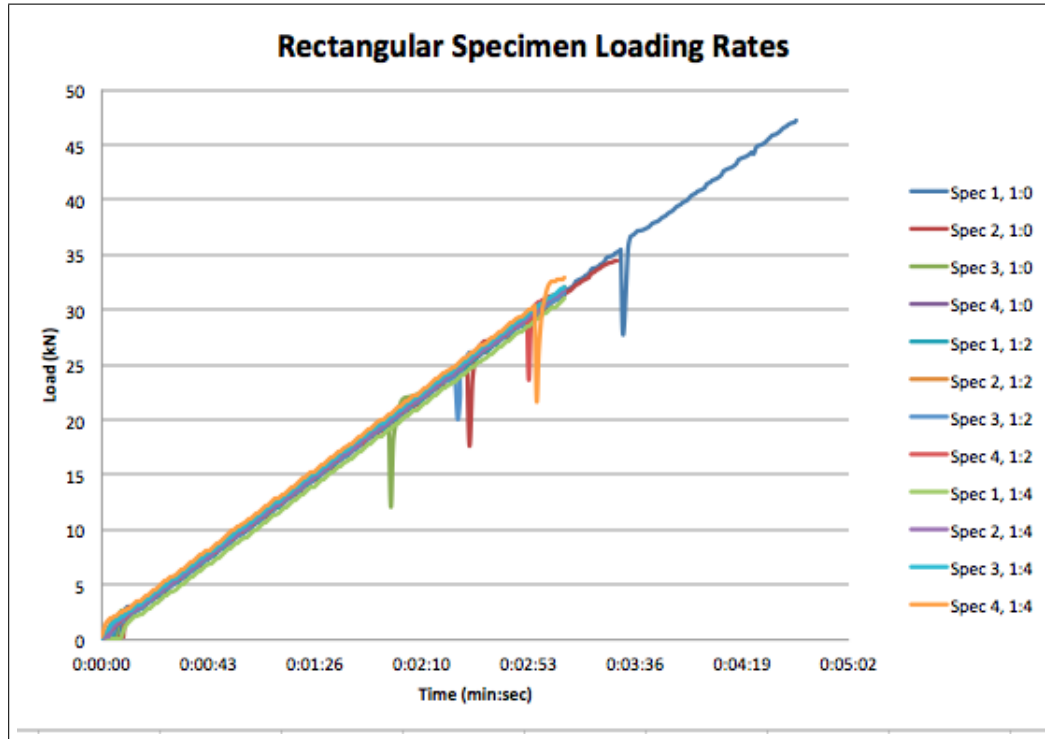


Figure 29: Load rates for rectangular specimens

It can also be seen from Figure 29 that every specimen experienced an extreme drop in load at some point throughout the experiment. The reason for this was at first presumed to be due to the notch crack initiating at this point. However, when compared to the actual loads at which the notch crack initiates, see Table 7, the drop appears to take place at a higher load. Therefore, it is presumed that the extreme decrease in load is the point at which the notch crack fully propagates passed the centre of the beam. This explanation seems plausible as when the crack fully propagates, the member is essentially changing section, as the only part of the member taking the load, would be the remaining section above the crack, thus the reason for the sudden drop in load.

4.1.2 Failure Modes

Table 5 shows the water content and initial failure type of each specimen. From this it can be seen that the notch corner cracked on every specimen before ultimate failure occurred.

Table 5: Rectangular Specimen Water Contents and Initial Failure Locations

Notch Angle Slope	Specimen No.	Water Content (%)	Location of Initial Failure
1:0	1		Cracked at notch corner
1:0	2		Cracked at notch corner
1:0	3		Cracked at notch corner
1:0	4	19	Cracked at notch corner
1:2	1	14	Cracked at notch corner
1:2	2	16	Cracked at notch corner
1:2	3	16	Cracked at notch corner
1:2	4	13	Cracked at notch corner
1:4	1	19	Cracked at notch corner
1:4	2	15	Cracked at notch corner
1:4	3	18	Cracked at notch corner
1:4	4	18	Cracked at notch corner

It should be noted that the water contents for rectangular specimens 1, 2 and 3 of 1:0 notch were unable to be taken due to lack of required equipment.

Throughout all rectangular experiments, there was a definite pattern in the types of failure that occurred. The first sign of failure occurred at the notch corner, where a crack would appear. The crack would initiate by first opening perpendicular to the grain at the notch corner (notch failure mode 1), due to excessive tensile forces, which can be seen in Figure 30.

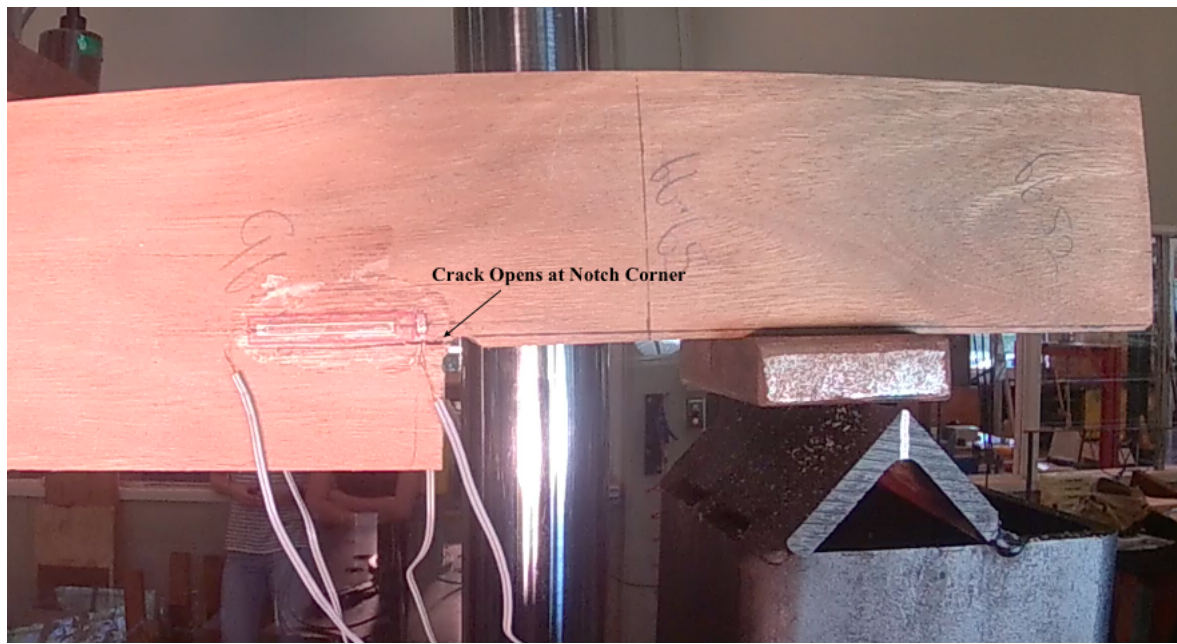


Figure 30: Specimen 4 notch 1:0, notch crack opening

The crack would then shear through the member (notch failure mode 2) and propagate to a point just beyond the centre of the beam, as seen in Figure 31. The notch corner crack then opened (failure mode 3) due to a combination of tensile and shear forces, which began after the crack initially sheared. This failure at the notch corner can also be clearly seen in Figure 31.



Figure 31: Specimen 4 notch 1:0, notch crack shearing and opening

After the notch crack had fully propagated passed the centre of the beam, the specimens ultimately failed in shear as can been seen in Figure 32.

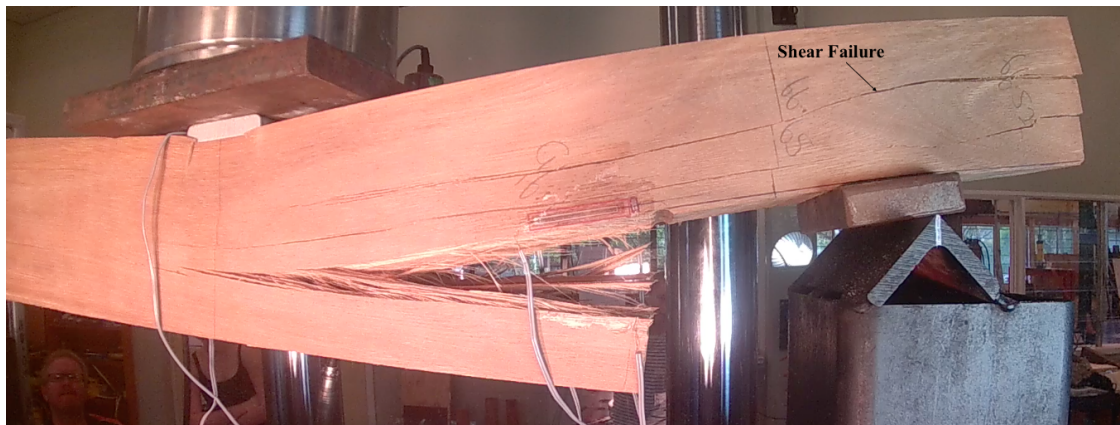


Figure 32: Specimen 4 notch 1:0, Shear Failure

Almost immediately after ultimate shear failure occurred, the specimens then failed in flexure at the centre of the beam, as shown in Figure 33. The overall succession of notch failure and ultimate failure occurred as expected; sequencing through the notch failure modes and ultimately failing in shear or flexure.



Figure 33: Specimen 4 notch 1:0, Flexural Failure

All rectangular specimens ultimately failed in shear and then flexure, apart from specimen 2 of the 1:0 slope notch, which only failed in flexure, as shown in Figure 34.



Figure 34: Specimen 2 notch 1:0 failure; side view left, top view right

As there was no obvious defects present on the specimen, we can only speculate on the reason why it did not fail in shear. A possible reason could be that the specimen may have had a very high water content at the centre of the beam significantly decreasing its flexural capacity in this region. This theory may be supported in Figure 35 where the specimen appears to be very wet in the specified area. However, as the water content was not taken for this specific specimen, this theory can not be verified.

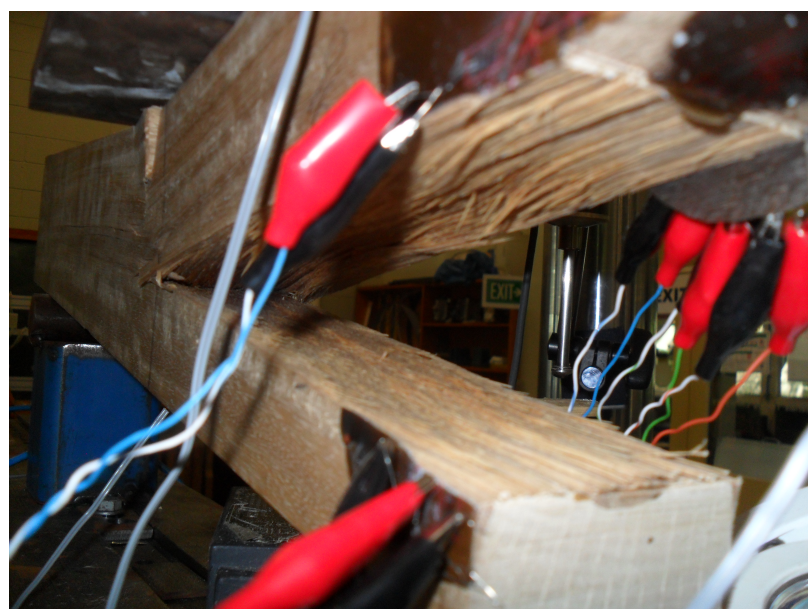


Figure 35: Specimen 2 notch 1:0; inside centre of beam

The ultimate shear failure occurred approximately through the middle of the cross-section of one half of the beam. However the location alternated between, over the notch half and over the roller support half (opposing end to the notch), throughout the experiments. A summary of these locations can be seen in Table 6.

Table 6: Rectangular Specimen Shear Failure Locations

Notch Angle Slope	Specimen No.	Shear Failure Location
1:0	1	Through section over roller support
1:0	2	N/A
1:0	3	Through section over roller support
1:0	4	Through section over the notch
1:2	1	Through section over the notch
1:2	2	Through section over the notch
1:2	3	Through section over the notch
1:2	4	Through section over roller support
1:4	1	Through section over the notch
1:4	2	Through section over the notch
1:4	3	Through section over the notch
1:4	4	Through section over roller support

A possible reason for the differing shear failures could be that, once the notch crack had sheared passed the centre of the beam and opened, the cross-section of the entire beam was reduced

to that over the notch. Hence the shear area and capacity became the same throughout the member, increasing the probability that it would fail at any point on the beam and differ due to each member's particular grain arrangement.

4.1.3 Ultimate Capacities

The overall capacities and times taken to for the failure to occur, for all rectangular specimens, are shown in Table 7. These results were determined through analysis of the load cell, LVDT and strain gauge data as well as through visual correlation using the footage taken of each specimen's notch and ultimate failures.

Table 7: Rectangular Specimen Crack Initiation and Ultimate Loads

Notch Angle Slope	Specimen No.	Notch Crack Initiation (kN)	Time for Notch to Crack (min:sec)	Ultimate Failure (kN)	Time to Ultimate Failure (min:sec)
1:0	1	30.11	02:58	47.16	04:41
1:0	2	23.88	02:22	34.39	03:29
1:0	3	16.08	01:33	27.97	02:46
1:0	4	23.27	02:18	41.94	04:12
1:2	1	26.89	02:39	42.56	04:14
1:2	2	21.53	02:03	39.77	03:57
1:2	3	23.65	02:20	33.40	03:23
1:2	4	29.24	02:52	40.20	04:22
1:4	1	38.46	03:52	41.79	04:14
1:4	2	49.23	04:51	49.23	04:51
1:4	3	36.80	03:35	39.04	03:49
1:4	4	29.84	02:52	34.51	03:20

From Table 7, it can be seen that the results for both the crack initiation capacity and the ultimate capacity vary substantially throughout the specimens for each notch slope. This is most likely due to a combination of differing water contents within the specimens and any

existing defects. When the results from this table are compared with the water contents, see Table 5, it can be observed for most specimens that those with a higher water content yield a lower ultimate capacity. This pattern is relevant to all specimens for notch slopes 1:2 and 1:4 except for specimen 1 of 1:4 notch, which yielded a slightly higher capacity than those of a lower water content. This outlier may be due to specimens 3 and 4 having defects, thus reducing their capacity. A defect was observed for specimen 4 but no surface defect was observed for specimen 3, see Appendix A. Another reason for this may be due to an inaccurate water content reading of one of the specimens, or the differing grain arrangement within the specimens. For the 1:0 slope specimens, a pattern with the capacity and water content was unable to be established as the water content was not taken for the first three specimens. However, when observing the specimen characteristics, given in Appendix A, it can be observed all specimens had different defects, thus would be expected to yield various capacities. As for the notch capacities, the same trend was apparent, where the higher the water content, the lower the capacity. Again, the capacities differed due to existing defects and their location, for example specimen 3 of 1:0 slope yielded particular low capacities, having a 15mm deep crack on top of the specimen, over the notch that spanned to the centre of the beam. The same discrepancy occurred with specimen 1 of 1:4 slope, where it yielded a higher notch capacity than those with a lower water content. This is indicative that the water content for this specimen may be inaccurate.

A graph summarising the information given in Table 7 is shown in Figure 36, where the solid bars indicate the average capacity and the error bars show the variance in the results. From this graph, there is a strong trend showing that both the crack initiation capacity (crack opening load) and ultimate capacity increase with increasing notch slope. The ultimate capacity experiences a gradual but significant average increase of 1kN between 1:0 and 1:2 slope and 2kN between 1:2 and 1:4 slope.

The same trend is observed for the notch capacities, however there is a more dramatic increase between the average notch capacity of a 1:2 slope and a 1:4 slope; where the difference between a 1:0 and 1:2 slope notch capacity is 2kN and between a 1:2 and 1:4 slope is 13kN. There was a large amount of variance in the results, however this large increase between these notch capacities would support AS1720 and TMR's recommendation to use a 1:4 slope as it appears

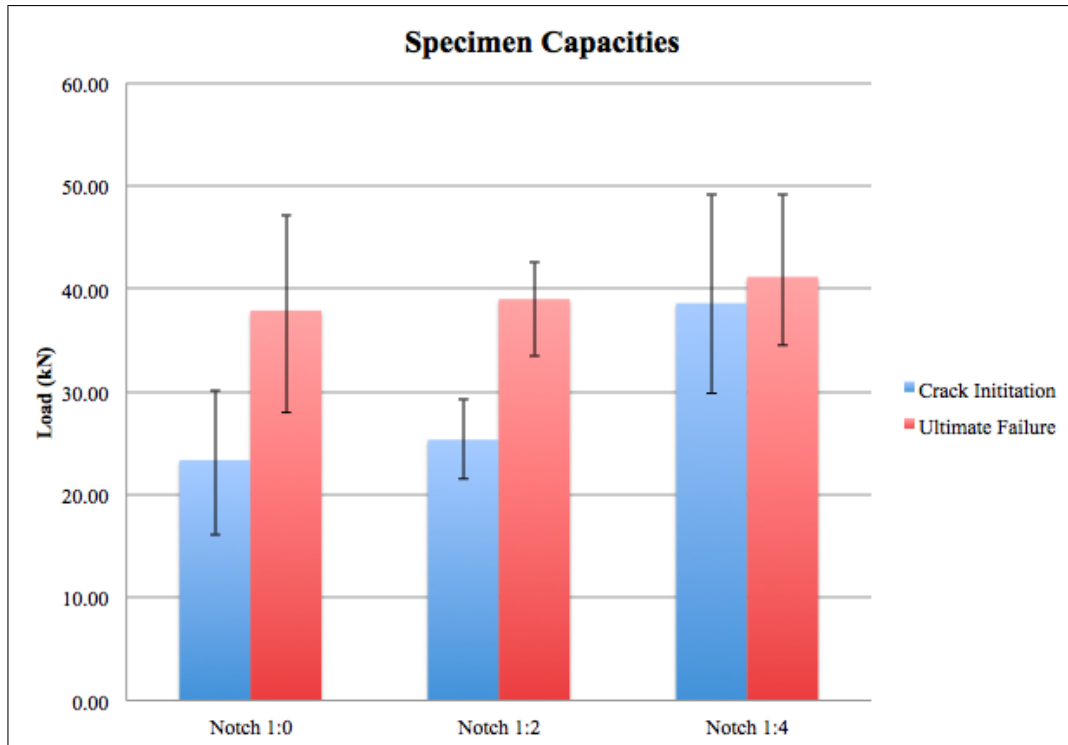


Figure 36: Capacities for Rectangular Section Specimens

to significantly improve the notch capacity.

The overall trend that can be observed in Figure 7 supports the common theory that a notch which is chamfered will have a greater capacity than a rectangular end notch (slope 1:0), and thus the critical notch angle for a rectangular section beam is a 1:0 slope.

Another relationship taken from the results in Table 7 can be seen in Figure 37, which shows the time between the notch crack initiating and ultimate failure. The bars in Figure 37 represent the average time interval for each notch slope and the error bars shows the variance in the results.

From this graph, it can be seen that there is an increase of 1 second between the 1:0 slope and 1:2 slope notch. This slight increase in time may be indicative of an average pattern or may be due to the average water content in the 1:2 slope notch being greater than those in the 1:0 slope. Unfortunately this theory can be neither denied or confirmed due to the unknown water contents for the 1:0 slopes, thus the reason for this increase in time interval is ultimately unknown. The most interesting trend observed from Figure 37 is that time average interval for the 1:4 slope notch is over a minute less than for the 1:0 slope and 1:2 slope, with an average of 16sec. This is not unexpected as it can be seen from Figure 36, that by the time the notch

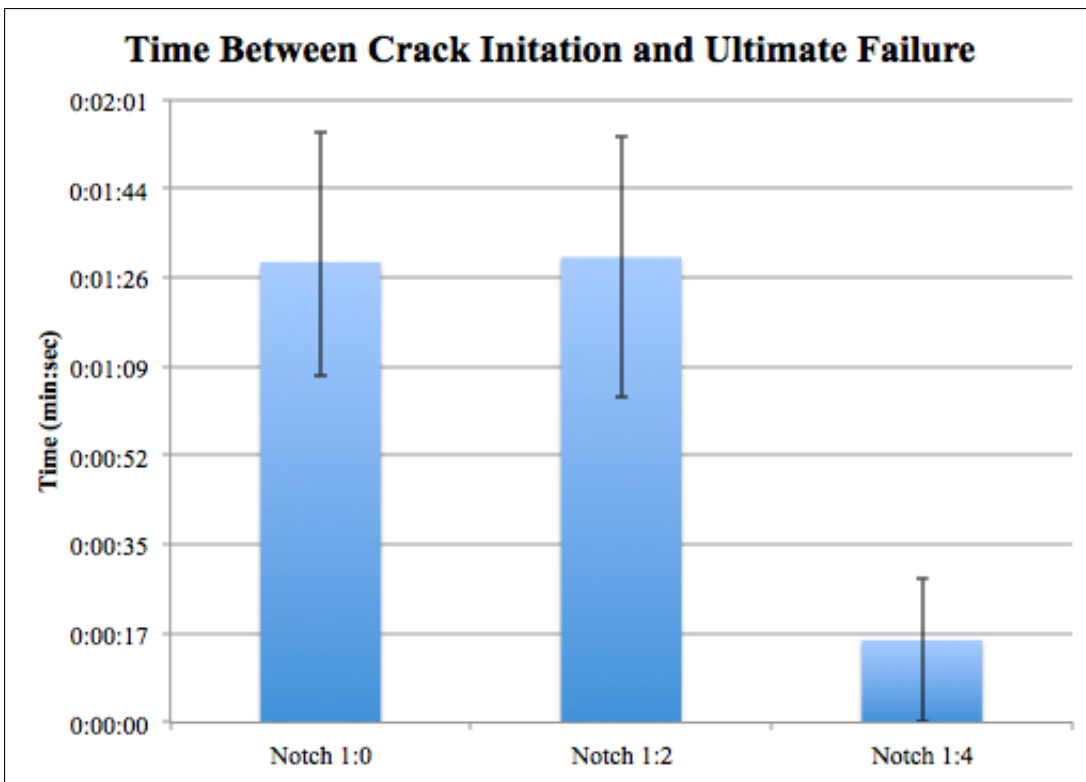


Figure 37: Time between notch initiating and ultimate failure for rectangular section specimens

crack initiates, the specimen is almost at ultimate capacity. Thus, this graphs shows that for a 1:4 slope notch on a rectangular beam, signs of cracking at the notch corner may indicate the member has reached, or is close to, ultimate failure. As this experiment was conducted under short-term loading, it is hard to specify the time interval between crack initiation at the notch and ultimate failure for a long-term load. Nevertheless research into the effects of long-term loading on the time between crack initiation at the notch corner and ultimate failure is warranted. This will determine if notching cracking is a sign of ultimate failure for 1:4 notch slope, and possibly alter current maintenance schemes for timber bridges.

4.1.4 Strain Gauge Analysis

All strain gauge data shown in the following graphs start from an applied load of zero and end at the point of ultimate failure or when the strain gauge cut out, whichever came first. It should also be noted than the additional weight from loading plates and loading cell has been taken into account. A strain gauge analysis is carried out below for each of the three differing notch slopes.

Notch Slope 1:0

The load-displacement graph from the LVDT results, for the rectangular section specimens, with a notch slope of 1:0 is shown in Figure 38.

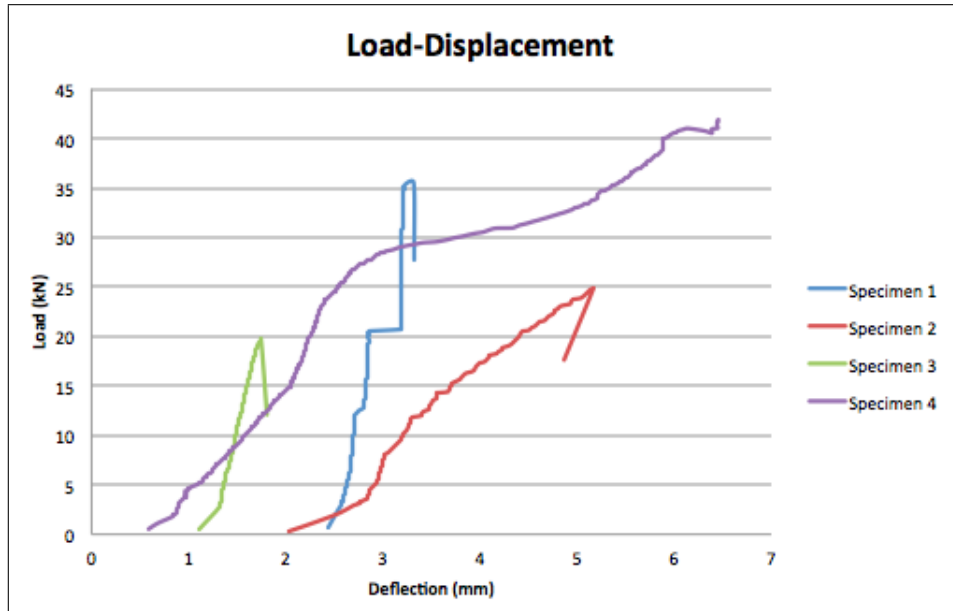


Figure 38: Load-displacement graph for rectangular beams with notch of slope 1:0

There does not appear to be any distinct trend in the load-displacement graph for specimen 1. This is assumed to be caused by the LVDT results being inaccurate from the plywood supporting the LVDT being too weak. As for specimens 2 and 3, the load-displacement graph gradually increases until it suddenly drops. This particular discrepancy is similar to that experienced in the loading chart, presumably due to the notch crack fully propagating through the specimen, and may be suggestive of this. The load-displacement graph for specimen 4 is uncommon in nature for no known reason.

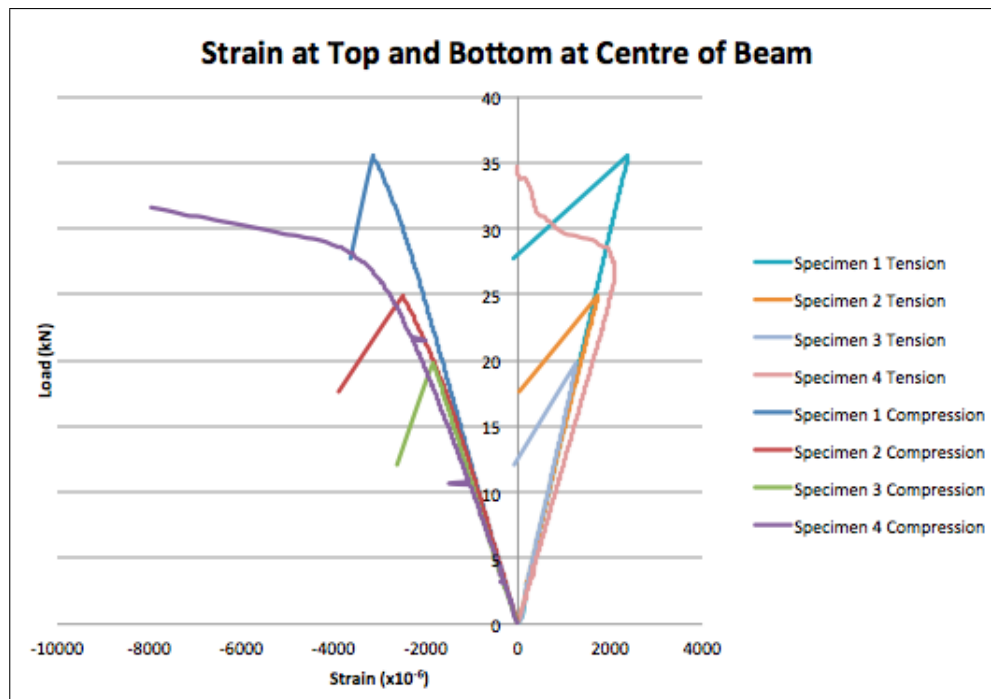


Figure 39: Top and bottom strain at centre for rectangular beams with notch of slope 1:0

The strains at the top (compressive) and bottom (tensile) of each specimen throughout loading are shown in Figure 39. It can be seen that specimens 1, 2 and 3 follow the same trend, where both tension and compression strains increase linearly and then suddenly drop at the same point. This sudden drop in load is suggestive of a sudden change in capacity and is assumed to be the point at which the notch crack fully propagates through the beam. Specimen 4 essentially followed the same trend, however there was no significant drop in the data, and instead experienced a smooth curve. This may be due to the notch crack propagating more gradually than the other specimens.

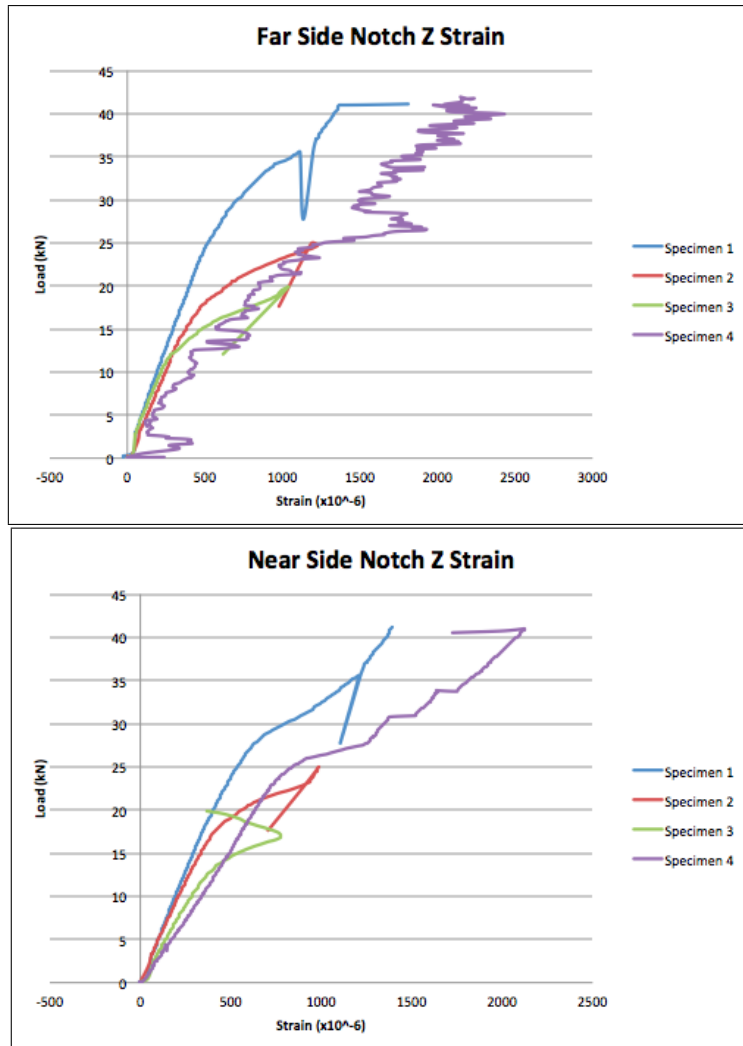


Figure 40: Horizontal strain either side of notch for rectangular beams with notch of slope 1:0

The horizontal strain at the notch corner for notches of slope 1:0 can be seen in Figure 40, where the horizontal strains were collected from either side of the notch and referred to as near side notch and far side notch, as per Figure 41. It can be seen specimens 1, 2 and 3 experience a similar strain on both sides of the notch, whereas specimen 4 experiences very erratic strain on the far side notch. The reason for this erratic strain may be due to frequent brittle fractures occurring along the notch crack, creating a nearly zig-zag effect.

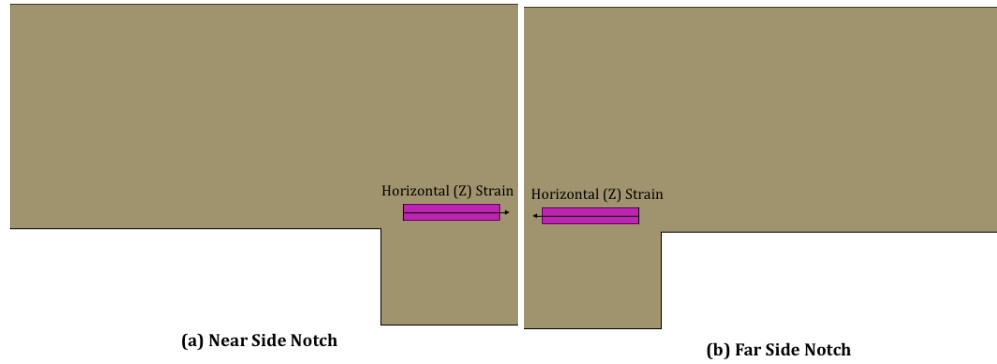


Figure 41: Z strain location and direction

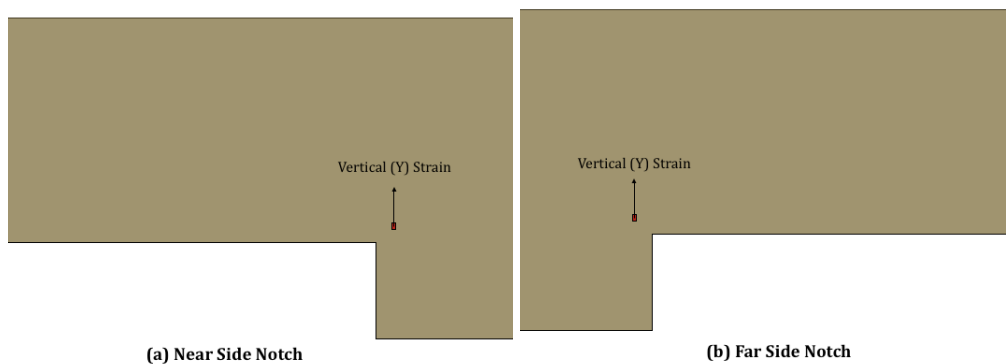


Figure 42: Y strain location and direction

The vertical strains were also taken from both sides of the notch, with the convention as shown in Figure 42. From the graphs in Figure 43, it is observed that the two sides experienced different patterns in the vertical strain at the notch corner. It can be seen for specimens 1 and 3 that at the point the strain passes zero on the near side notch, the strain experienced on the far side notch begins to plateau. This point aligns with the load at which the crack initiated. The reason both side experienced different pattern in strain is ultimately unknown.

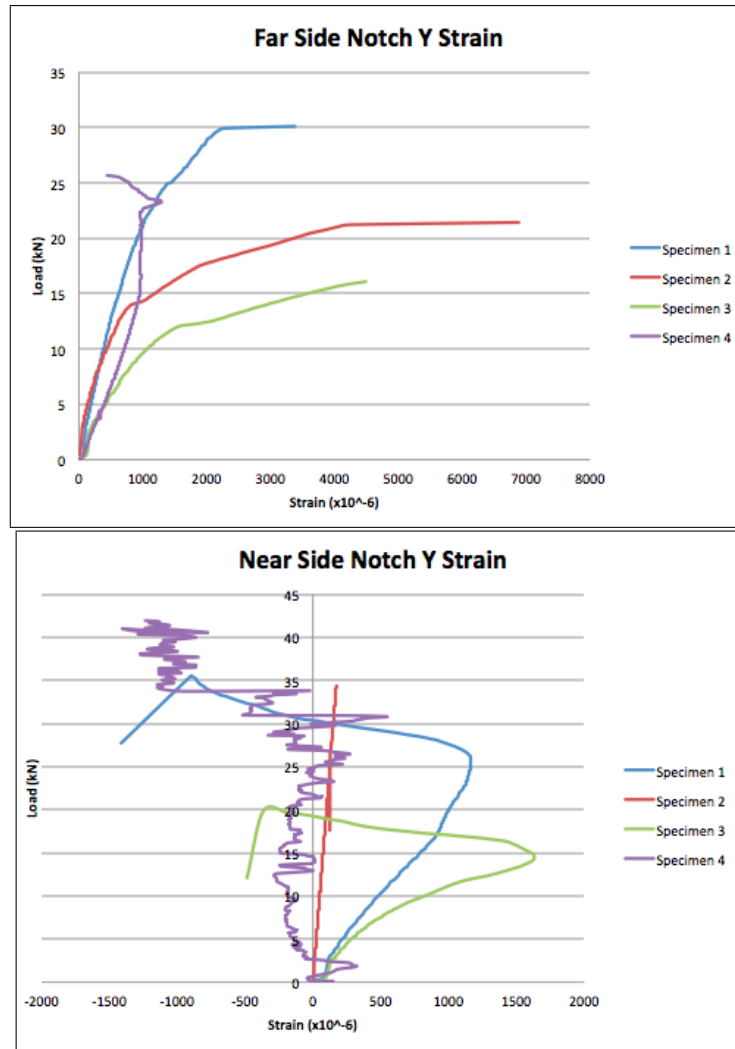


Figure 43: Vertical strain either side of notch for rectangular beams with notch of slope 1:0

Specimen 4 experienced erratic strain on the near side notch, again indicative frequent small fractures occurring along the notch crack. The vertical strain obtained for specimen 2 showed no distinct pattern on the near side notch which may be due to a large wedge cut out of the notched end of the beam, as shown in Figure 44. This wedge was likely in line with the strain gauge and obscured the data.



Figure 44: Rectangular specimen 2 notch slope 1:0; wedge defect

Notch Slope 1:2

The load-displacement graph for the 1:2 notch specimens follow the same distinct pattern distinguished in the 1:0 slope load-displacement graph, where the load increases until it suddenly drops at the point at which the notch crack is assumed to have fully propagated. This was seen for all specimens except specimen 2 which did not experience a drop and instead, curved at the crack propagation load, then continued to increase in an almost linear manner, see Appendix C.

The same trends were can be observed for the 1:2 slope tension and compression strains, as were for the 1:0 slope; where both strains spiked at the point at which the notch crack fully propagates, see Appendix C. Specimens 1, 3 and 4 followed this specified trend, where specimen 2 followed the same trend as specimen 4 for the 1:0 slope, again presumptively due to the crack growth being less sudden than the other specimens.

The horizontal strain data can be seen in Figure 45, where specimens 1, 3 and 4 roughly experience the same trend either side of the notch, dropping at the same point. This point is assumed to be where the crack fully propagated.

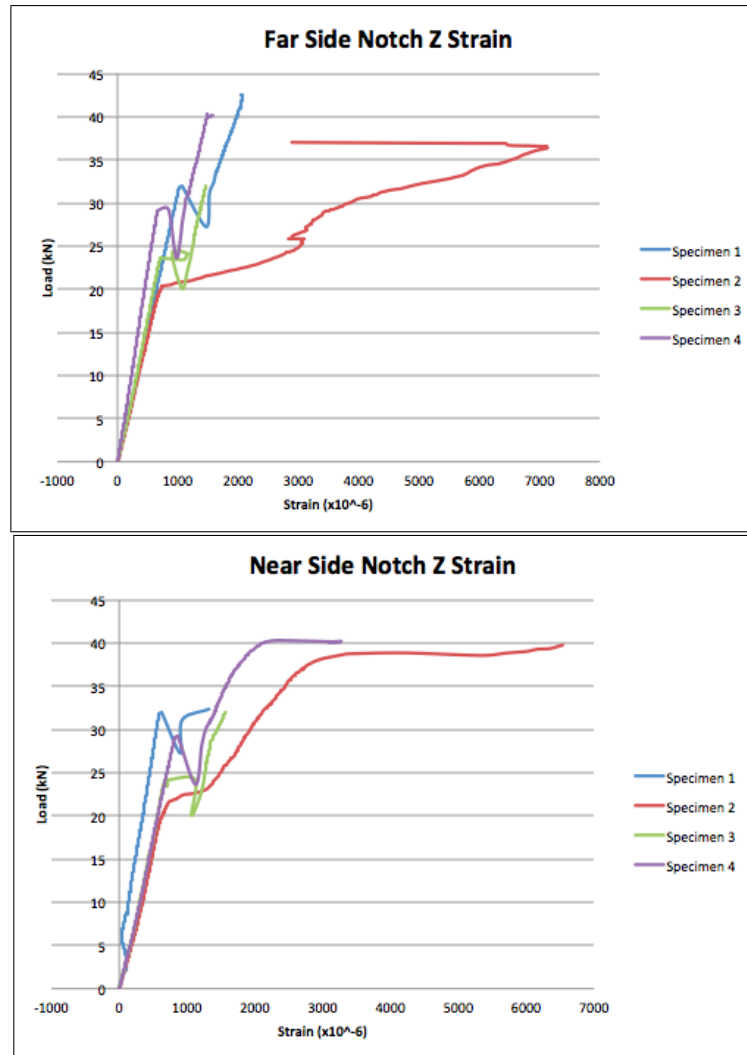


Figure 45: Horizontal strain either side of notch for rectangular beams with notch of slope 1:2

Whereas, the strain underwent by specimen 2 followed became erratic on the far side notch, after the notch crack initiated. This is most likely due to the large cut into the end of the specimen over the notch, see Figure 46, which would have interfered with the strain gauge data.



Figure 46: Rectangular specimen 2 notch slope 1:2; thick cut defect

The same was observed in the vertical strain as in the horizontal, where both sides of the notch follow similar trends except for specimen 1, which became erratic after notch crack initiation, see Appendix C. It was also observed that for the drop in the common trend for the vertical strains aligned with the crack initiation load.

Notch Slope 1:4

The load-displacement graph for the 1:4 can be seen in Figure 47. The same trend that was observed as for the previous experiments, where the graph gradually increases to a point. However, in the other experiments, the load would drop at this point, indicating the point at which the notch crack fully propagated, which only occurred in specimen 4. This drop did not occur in specimens 2 and 3 as the notch crack initiated at the point of ultimate failure. Whereas specimen 1 experienced a very different and unexpected trend. The reason for this unknown as there was no observed defects on the specimen before testing, but there may have been internal defects that were not accounted for.

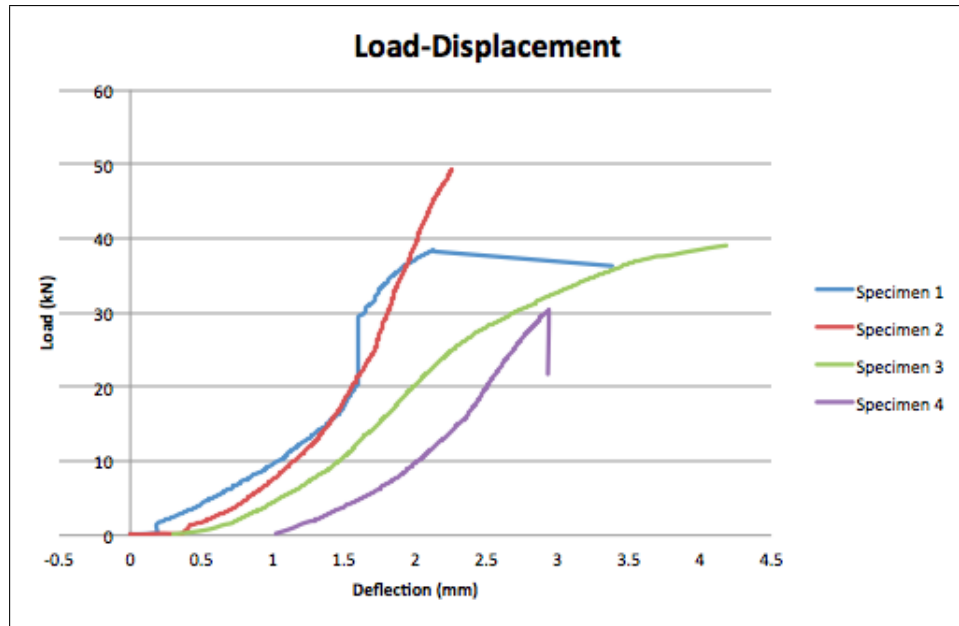


Figure 47: Load-displacement graph for rectangular beams with notch of slope 1:4

The same trends for the top and bottom strains at the centre of the beam were experienced for the 1:4 slope specimens as both the 1:2 and 1:0 slope specimens, see Appendix C. Except, specimens 2 and 3 did not experience a sudden drop in strain as the notch crack did not fully propagate before ultimate failure.

The horizontal strain followed the exact same linear pattern on either side of the notch, see Appendix C, where only specimens 1 and 4 experienced a sudden drop/plateau at the point of notch crack initiation. The vertical strains experienced by the 1:4 notch specimens can be seen in Figure 48. These strains overall follow the same linear trend, However, specimen 1 suddenly decreases in strain at the point of crack initiation in both graphs. The strains for specimens 3 and 4 cannot be compared either side of the notch as the strain gauges malfunctioned.

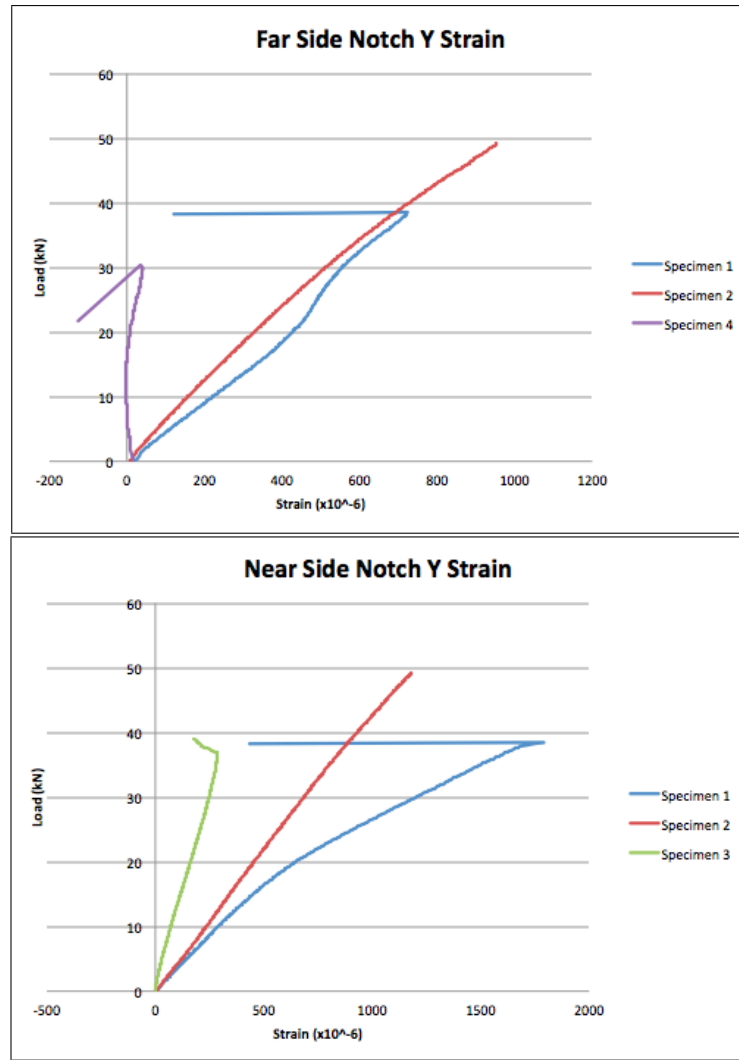


Figure 48: Vertical strain either side of notch for rectangular beams with notch of slope 1:4

4.2 Round Specimens

4.2.1 Loading Rates

The loading rates used for the round specimens can be seen in Figure 49. The load rate was constantly 10kN per minute for all specimens, except for specimens 1 and 3 for notch slopes 1:0, which experienced a load rate of 8kN per minute. This error in loading rate was due to an error in the MTS loading settings which was fixed for the rest of the experiments.

The same extreme drop in load occurred in most of the round specimens as did in the rectangular specimens, however were less prominent (i.e. less of a decrease) than those present in Figure 29. Another difference between the round and rectangular specimen loading graphs were that some of the round specimens did not experience an extreme decrease in load. As it

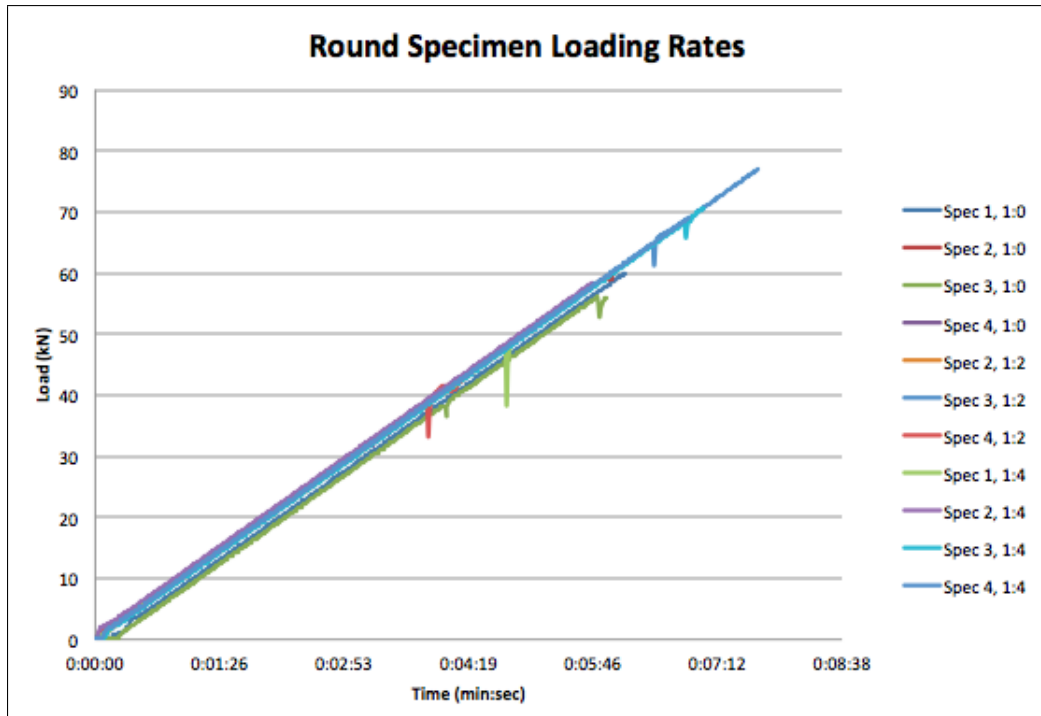


Figure 49: Load rates for round specimens

was presumed for the rectangular specimens that the decrease was due the notch fully propagating, it would be safe to assume the same for the round specimens, where the ones that didn't experience a drop, did not crack at the notch corner.

It should also be noted that specimen 1 of notch slope 1:2 was unable to be plotted on this graph as the load cell malfunctioned during the loading and the load was then taken from the MTS. The load data collected from the MTS machine was taken at slightly different load points than the data taken using the data logger, thus the loads and times were unable to be exactly aligned. However, the MTS was set to load this specimen at a rate of 10kN per minute.

4.2.2 Failure Modes

Table 8 shows the water contents of the round specimens and their initial modes of failure. As it can be seen, not all specimens initially failed at the notch corner. Specimens 1 of 1:0 slope and 2 of 1:4 slope initially failed at a different location due to existing defects. Whereas specimen 4 of 1:4 slope did not fail at the notch corner until ultimate failure occurred.

Table 8: Round Specimen Water Contents and Initial Failure Locations

Notch Angle Slope	Specimen No.	Water Content (%)	Location of Initial Failure
1:0	1	22	Cracked propagated from existing crack at opposite end, then cracked at notch corner
1:0	2	21	Cracked at notch corner
1:0	3	24	Cracked at notch corner
1:0	4	26	Cracked at notch corner
1:2	1	23	Cracked at notch corner
1:2	2	30	Cracked at notch corner
1:2	3	22	Cracked at notch corner
1:2	4	29	Cracked at notch corner
1:4	1	24	Cracked at notch corner
1:4	2	22	Cracked propagated half way down chamfer, then cracked at notch corner
1:4	3	27	Cracked at notch corner
1:4	4	23	Notch cracked at ultimate failure

The exact failure mode for the round specimen is not as clear as it was for the rectangular specimens. As can be seen in Table 9, the round specimens generally failed in flexure at the centre of the beam, however there were some that failed in shear. The reason for this is presumed to be due to defects effecting the shear capacity. It was noted that a large number of defects were present on the round specimens before testing, see Appendix B, and it is highly likely that defects were present within the specimens that were not accounted for, such as internal rot.

Table 9: Round Specimen Ultimate Failure Modes

Notch Angle Slope	Specimen No.	Shear Failure Location
1:0	1	Shear failure due to existing defect
1:0	2	Flexural failure
1:0	3	Failed in shear through notched end
1:0	4	Flexural failure
1:2	1	Flexural failure
1:2	2	Flexural failure
1:2	3	Failed in shear over opposing end to notch
1:2	4	Failed in shear through opposing end to notch
1:4	1	Failed in shear through existing rot, over notched end
1:4	2	Flexural failure
1:4	3	Flexural failure
1:4	4	Flexural failure

In most cases, the specimens followed the three modes in notch cracking as predicted; where a crack would first open and the notch corner (mode 1) and then shear (mode 2), as can be seen in Figure 50.



Figure 50: Specimen 2 notch 1:2, notch crack shearing and opening

The notch crack would then gradually propagate to roughly the centre of the beam when the notch crack fully opens and flexural failure occurs, as shown in Figure 51.

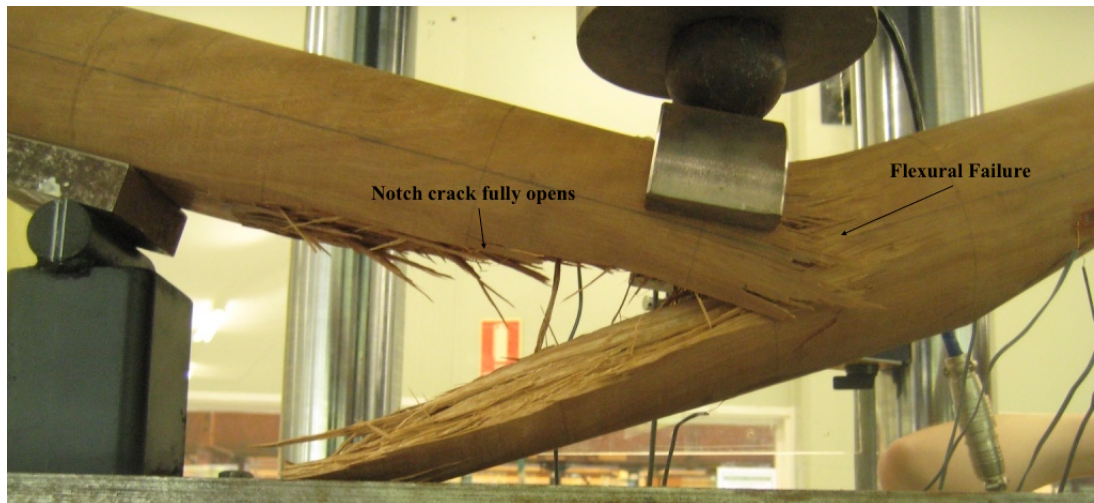


Figure 51: Specimen 4 notch 1:4, notch crack fully opening and ultimate failure

The notch crack propagation was found to be a lot more gradual compared to the rectangular specimens, which occurred almost instantaneously. Due to this, the time between the notch crack fully propagating and ultimate failure was shorter for the round specimens than the rectangular.

Specimen 1 of 1:0 slope notch failure was unexpected and different from any other specimen

failure throughout this experiment. The specimen de-laminated from an existing knot, shown in Figure 52, located on the small notched support section, over the roller support.



Figure 52: Specimen 1 notch 1:0, existing knot at small notched section over roller support

This de-lamination gradually sheared through the grain, when the notch corner then cracked and also began to propagate. However, the notch crack did not propagate more than 5cm nor get to mode 3. Instead a shear crack began to form over the notch corner, which can be seen in Figure 53. Once the de-lamination crack propagated to about mid-way through the member, small shear cracks appeared along the specimen, the crack over the notch began to open, and the member ultimately failed in shear.

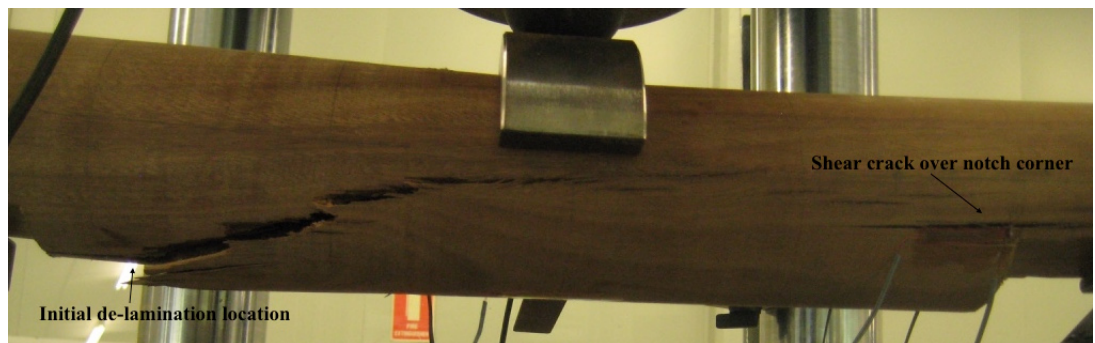


Figure 53: Specimen 1 notch 1:0, final failure

The shear failure that occurred in the remaining specimens followed the exact same process as

seen for the rectangular specimens. Again, there was no obvious reason to the location of the shear failure, except for specimen 1 of slope 1:4, which sheared through existing rot.

4.2.3 Ultimate Capacities

The loads and times at which each specimen underwent notch failure and ultimate failure is shown in Table 10. The results are even more variable throughout each notch slope experiment than the rectangular specimens. The reason for this is presumed to be due to the round specimens having significantly more defects than the rectangular specimens.

Table 10: Round Specimen Crack Initiation and Ultimate Loads

Notch Angle Slope	Specimen No.	Notch Crack Initiation (kN)	Time for Notch to Crack (min:sec)	Ultimate Failure (kN)	Time to Ultimate Failure (min:sec)
1:0	1	53.50	05:20	59.98	06:00
1:0	2	44.46	04:25	60.06	05:59
1:0	3	36.23	03:49	55.91	05:55
1:0	4	22.76	02:15	36.62	03:38
1:2	1	47.68	03:48	61.83	04:57
1:2	2	47.05	04:41	53.42	05:19
1:2	3	64.65	06:26	76.94	07:40
1:2	4	38.92	03:50	42.99	04:18
1:4	1	47.56	04:45	49.11	04:50
1:4	2	58.48	05:46	58.48	05:46
1:4	3	65.76	06:50	70.69	07:03
1:4	4	69.01	06:52	69.01	06:52

There is a slight pattern between the water content and the and the failure capacities; where a higher content yields a lower capacity. This is prominent in the ultimate failure capacities for the 1:0 and 1:2 slope specimens, but the 1:4 slope data does not comply with this trend. As for the notch crack capacity, the same somewhat trend is present throughout the experiments,

except for specimen 1 of notch slope 1:0, which failed in a different location prior to cracking at the notch corner. Although there is a slight pattern in the capacity in relation to the water contents, the amount of defects present during testing make it difficult to verify this trend.

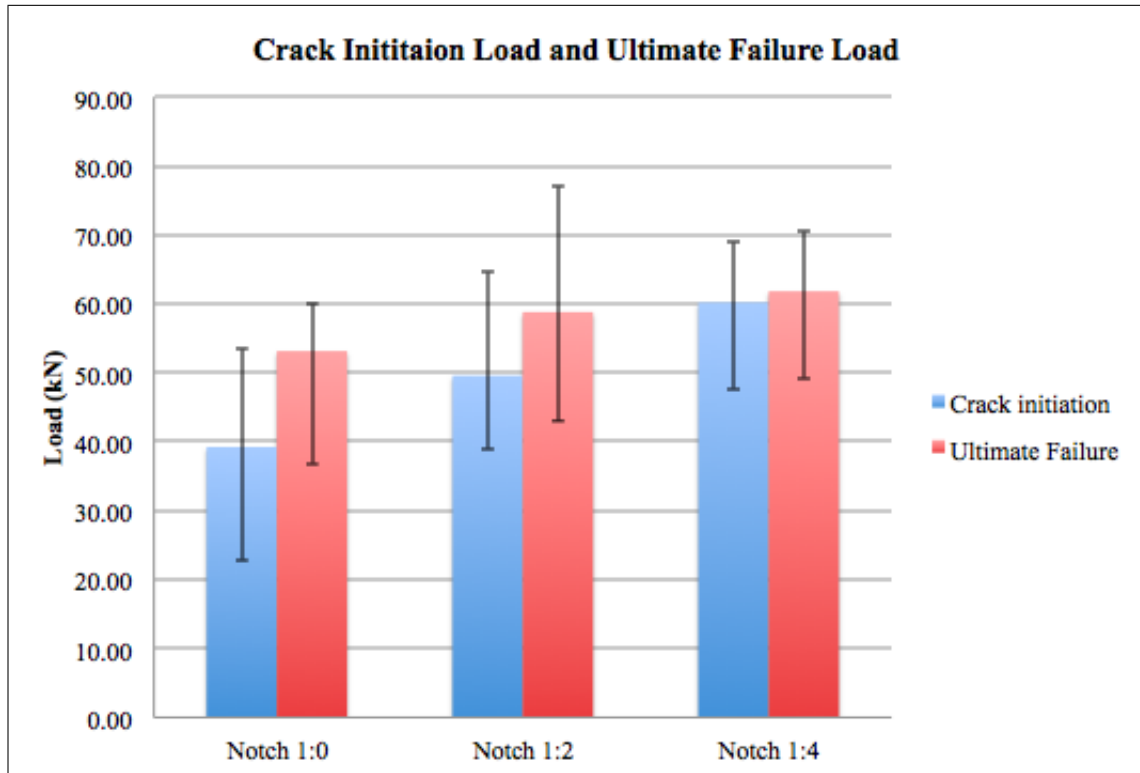


Figure 54: Capacities for Circular Section Specimens

The capacities given in Table 10 were graphed for each notch slope and displayed in Figure 54, where the bars indicated the average capacities and the error bars show the variance in the results. From this graph, it is observed that the ultimate capacity increases with an increasing notch slope. The difference between the average ultimate capacities for the 1:0 and 1:2 slope specimens is slightly greater than that for the 1:2 and 1:4 specimens, being 5.6kN and 3.0kN respectively. This is most likely due to the two of the 1:0 slope specimens being loaded at a slightly slower rate, which effect is unknown on the capacity. A more distinct increase and trend is observed for average notch capacity, through the increasing notch slopes; with a difference of 10.3kN and 10.6kN respectively. Overall, it is determined that a 1:0 slope notch yields the lowest capacities and thus is the critical notch angle for the round specimens.

Figure 55 shows the time between the crack initiating at the notch corner and ultimate failure

for the round specimens.

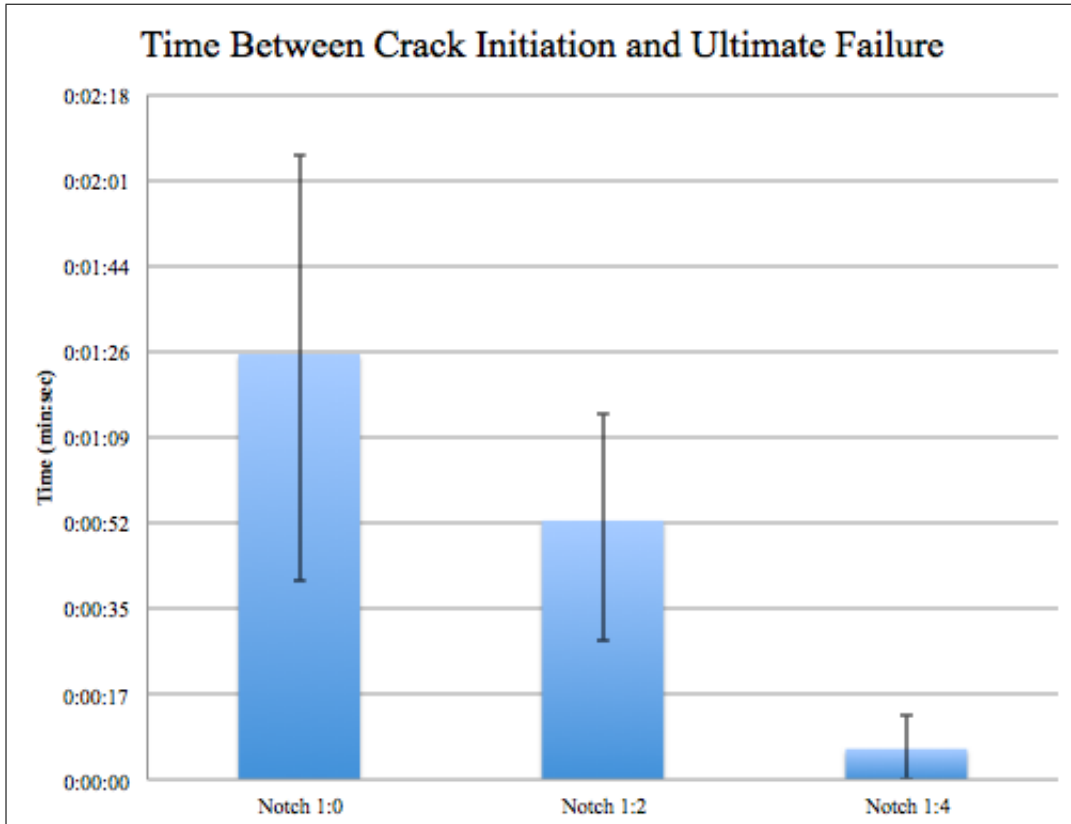


Figure 55: Time between notch crack initiation and ultimate failure

From this graph, a distinct trend can be observed, where the time between the notch cracking and ultimate failure significantly decreases with an increasing notch slope. This was not unexpected, as it appears from previous results that the increase in notch slope increases the capacity of the notch, thus the load at which the notch cracks is getting closer to the ultimate capacity of the beam. As discussed for the rectangular specimens, these results could show that a round member notched with a 1:4 slope notch that is showing signs of notch cracking may be reaching its ultimate capacity.

4.2.4 Strain Gauge Analysis

Due to the curvature of the specimens, the strain gauges experienced some initial strain before loading began. To account for this, the strain gauges were zeroed before loading commenced (i.e. at a load of zero).

Notch Slope 1:0

The load-displacement data collected from the LVDT is given in Figure 56 for all four round specimens with a notch slope of 1:0.

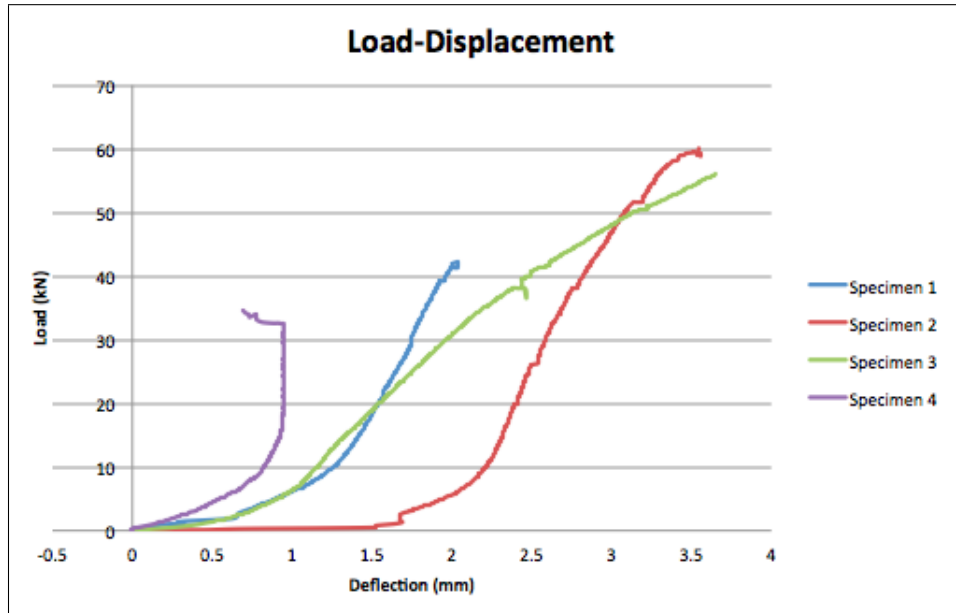


Figure 56: Load-displacement graph for round beams with notches of slope 1:0

The load-displacement graphs for specimens 1, 2 and 3 roughly follow the trend established for the rectangular specimens, except specimen 1 becomes erratic at around 42kN load. This odd behaviour displayed by specimen 1 is presumed to be correlating with the initiation of the de-lamination from the existing knot as discussed earlier. The load-displacement for specimen 4 does not follow the standard trend and the reason for this be related to an issue with the LVDT or an existing defect. Overall, these graphs appear to be significantly smoother than those for the rectangular specimens, which is assumed to be due to the notch cracks propagating more gradually in the round specimens than the rectangular.

The compressive strain at the top and tensile strain at the bottom in the centre of the beam is shown in Figure 57, where it was graphed against the applied load. Specimens 2, 3 and 4 experience an increasing linear trend in both compression and tension until they suddenly plateau.

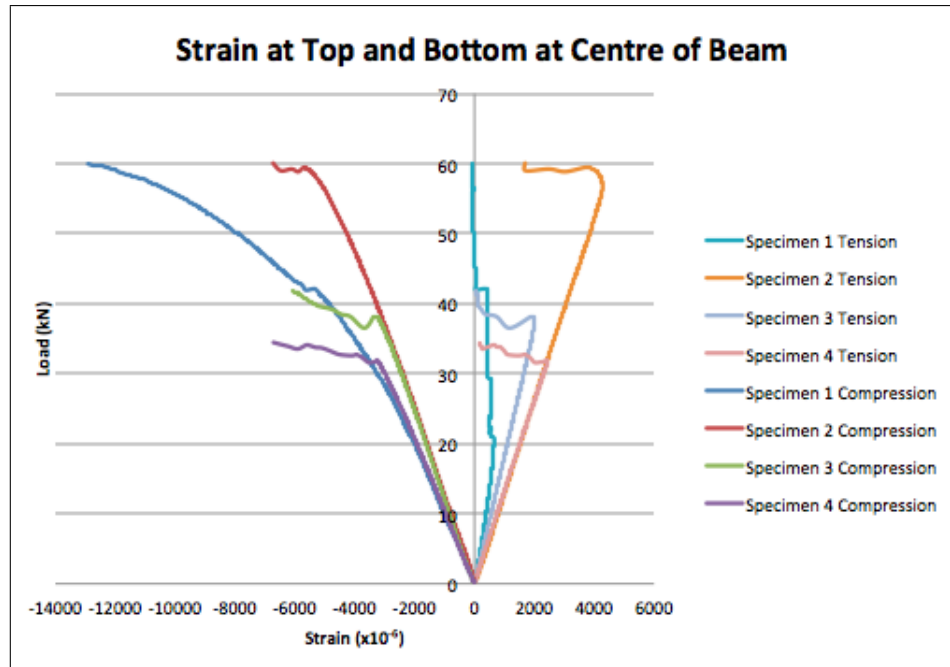


Figure 57: Top and bottom strain at centre for round Beams with notches of slope 1:0

The point at which the graph plateaus is assumed to be caused by the notch crack fully propagating. Specimen 1 follows slightly different trends in both compression and tension, which is most likely due to the initial crack occurring due to the existing defect, on the opposing end to the notch.

The horizontal strain either side of the notch corner with relation to the applied load is shown in Figure 58. It is observed that all specimens horizontal strains linearly increase until they reach a point where they begin to curve, except specimen 1 far side notch which suddenly drops in strain. This point of curvature or drop aligns with the notch crack initiating. It should also be noted that the fair side notch strain gauge for specimen 4 malfunctioned.

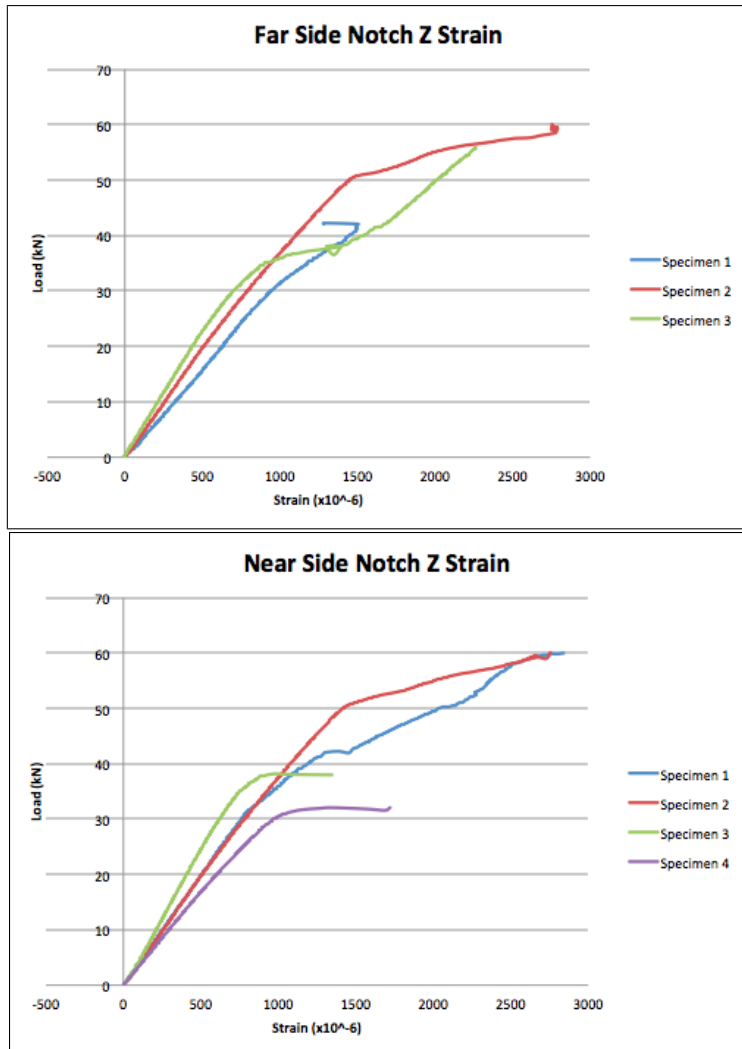


Figure 58: Horizontal strain either side of notch for round beams with notch of slope 1:0

The vertical strain either side of the notch corner with relation to the applied load is shown in Figure 59. It can be seen that specimens 1, 2 and 3 follow roughly the same pattern; where they linearly increase, begin to plateau and then change direction. Unlike the rectangular specimens, there does not seem to be a clear reason for this trend and it is hard to distinguish where the notch crack initiated in this data. Specimen 4 follows a different trend on the near side notch which is assumed to be due to an existing crack running through the centre of the notched section, see Appendix B for details.

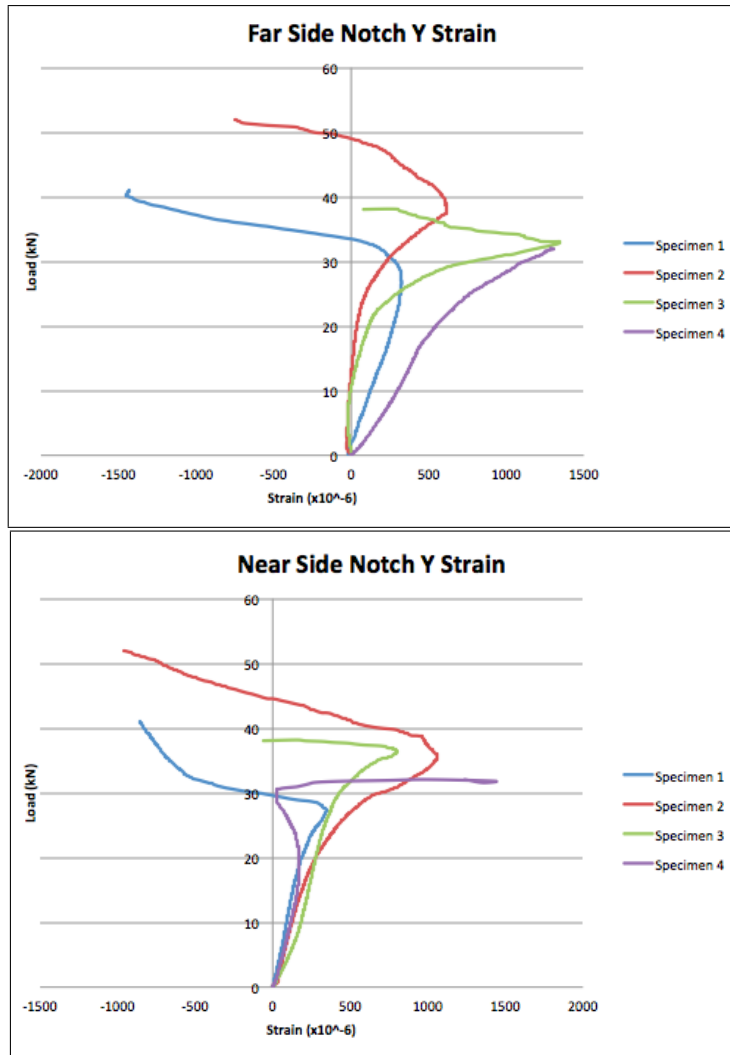


Figure 59: Vertical strain either side of notch for round beams with notch of slope 1:0

Notch Slope 1:2

The load-displacement graphs for all specimens with a 1:2 slope notch roughly followed the standard trend, see Appendix C. The compressive and tensile strains at the centre of the beam can be seen in Figure 60. This graph shows the compressive and tensile strain experienced by the 1:2 slope specimens had a pattern similar to that experienced by the rectangular specimens; with a more distinct decrease in strain. This decrease correlates to the point at which the notch crack initiates. The graph from Figure 60 indicates the notch crack initiation was more abrupt in the 1:2 slope specimens than was in the 1:0 slope specimens.

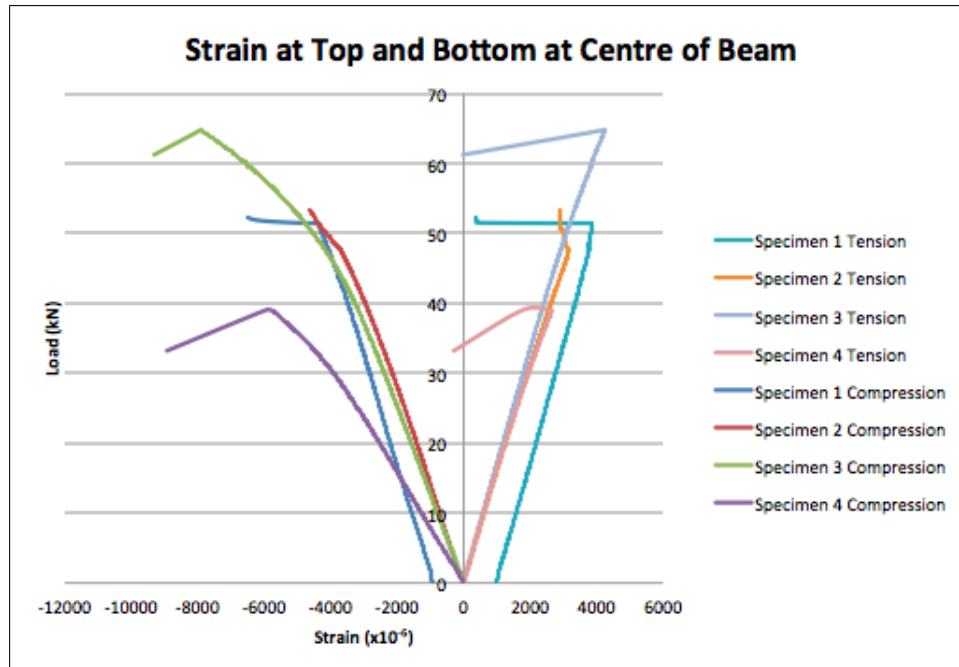


Figure 60: Top and bottom strain at centre for round beams with notches of slope 1:2

The horizontal strains either side of the notch corner were observed to follow roughly the same trend, and can be seen in Appendix C. The vertical strain for the 1:2 slope specimens are shown in Figure 61. Both these graphs follow a linearly increasing trend until they hit a point where they suddenly plateau. This point at which each graph changes from the linear trend correlates with the load at which the notch crack initiates. Thus, this supports the earlier statement that the crack initiation is more abrupt than for the 1:0 slope sound specimens.

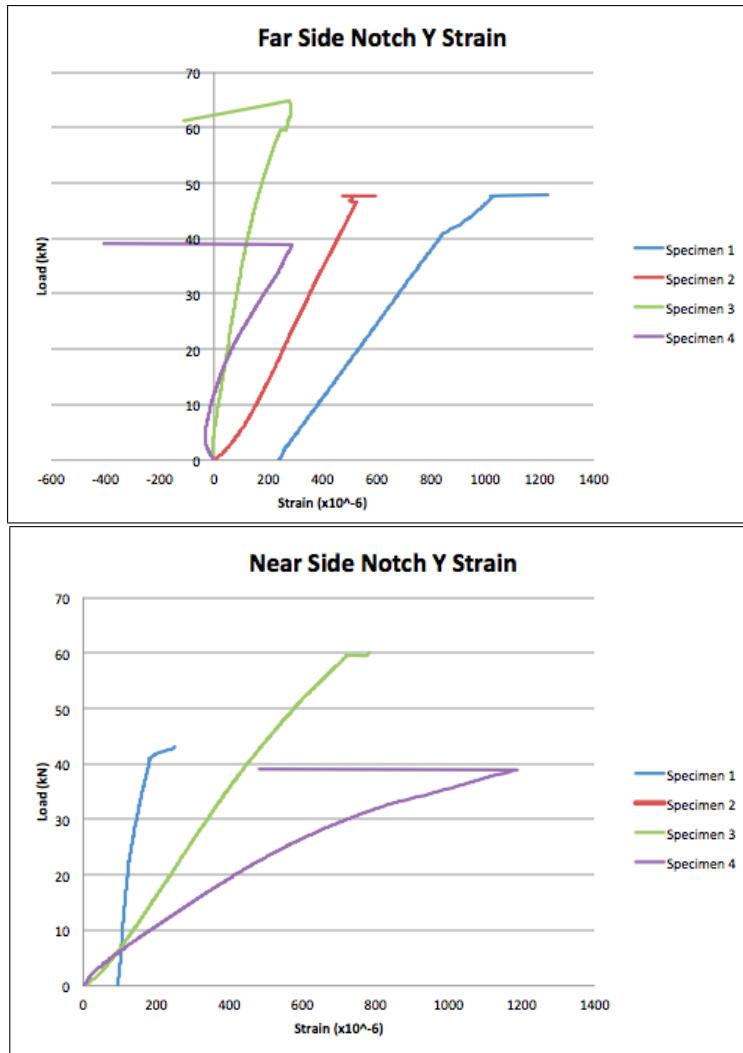


Figure 61: Vertical either side of notch strain for round beams with notch of slope 1:2

Notch Slope 1:4

The load-displacement graph for specimens 2, 3 and 4 of 1:4 slope notch round specimens followed the standard trend, but specimen 1 followed the same trend as experienced by specimen 4 of 1:0 slope, see Appendix C. This difference in trend for specimen 1 is assumed to be due to the large amount of drying cracks and knots present before testing, see Appendix B.

The compressive and tensile strain experienced by all specimens followed the exact same trend as experienced by the 1:2 slope round specimens; where the sudden drop in the trends align with the load at which the notch crack initiates. See Appendix C for slope 1:4 round specimen compressive and tensile strain at beam centre graph.

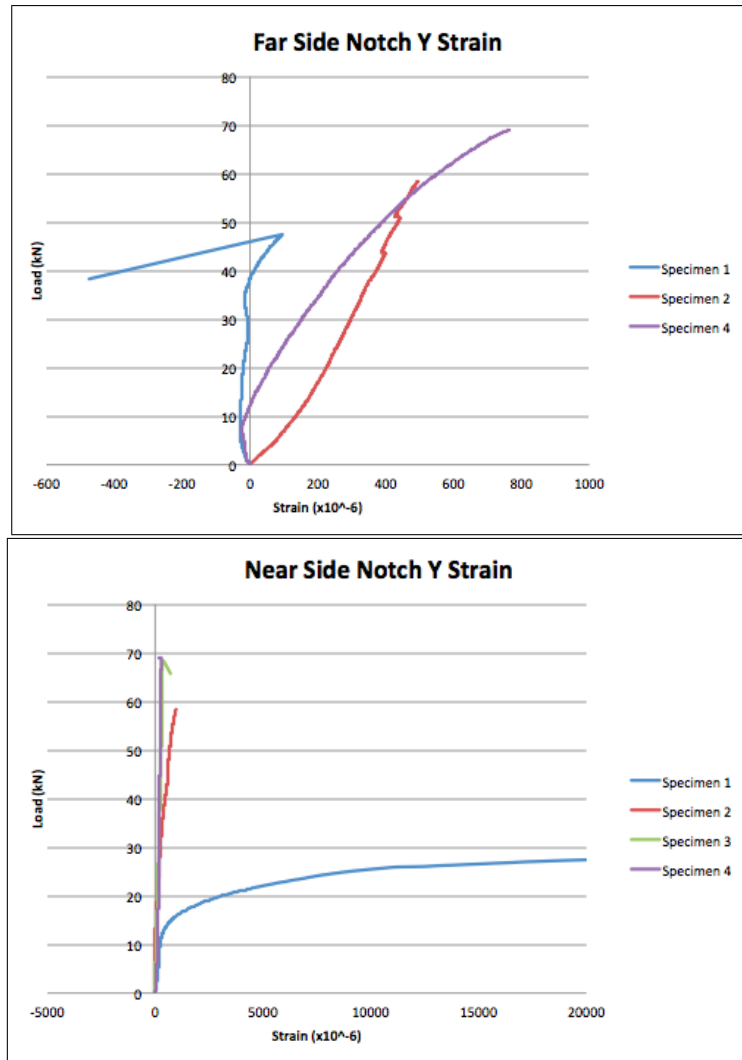


Figure 62: Vertical either side of notch strain for round beams with notch of slope 1:4

The horizontal strains follow the same trend either side of the notch, as observed throughout the other experiments. The vertical strains experienced by the 1:4 round specimens through the notch corner can be seen in Figure 62. Specimens 2 and 4 follow the similar trends either side of the notch, and specimen 3 had a malfunctioning strain gauge on the far side notch. Specimen 1 experienced significantly different strain trends either side of the notch, assumed to be due to the large amount of existing defects present.

4.3 Comparison of Round and Rectangular Section

The main difference observed between the circular and rectangular section specimens was the general ultimate failure mode for the round specimens was flexural failure, where the rectangular members experienced shear failure. The reason for this is assumed to be due to the way the grain responds to the load between the two different cross-section, such as the shear failure

may be facilitated by the longitudinal grain in the rectangular profile. Another reason for this difference in failure modes may also be due to the round specimens having a larger section above the notch corner than the rectangular specimens.

Another difference that was noticed between the two sections was the notch propagation for the rectangular section happened almost instantaneously, whereas the notch crack tended to propagate very gradually through the circular section specimens. This is also presumed to be due the two different cross-sections respond to the load.

The graph presented in Figure 63 shows the average ultimate capacities graphed with respect to the angle of the notch chamfer, from the notch corner. It is observed that the overall trend for both sections is very similar, with the round specimens yielding a slightly greater initial incline than the rectangular members. However, this may be due to the circular section having a greater response to the increase in slope angle, or it could be due to two of the 1:0 slope specimens being loaded at a slightly slower rate.

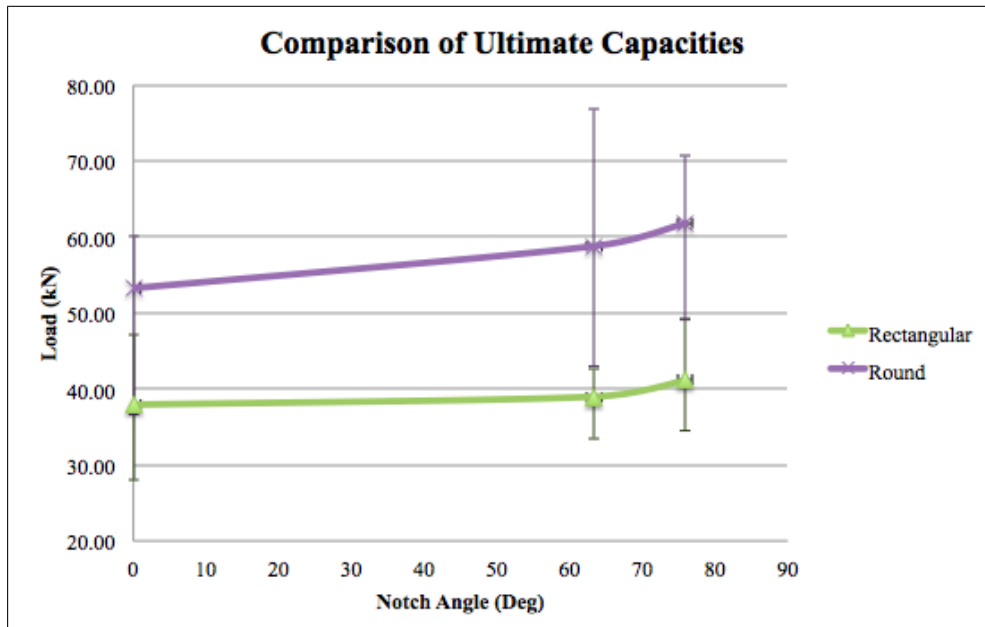


Figure 63: Comparison of rectangular and circular section ultimate capacities

The average notch initiation capacities in relation to the angle of the slope from the notch corner can be seen in Figure 64. Both the rectangular and round specimens yield similar trends, and similarly the incline between the 1:0 and 1:2 slope notch is greater for the round than the rectangular specimens. However, the notch capacities for the rectangular specimens seem to

respond more to the increase in notch angle than the round specimens. The reason for this is unknown, but is presumed to be due to the way the two section types respond to the load.

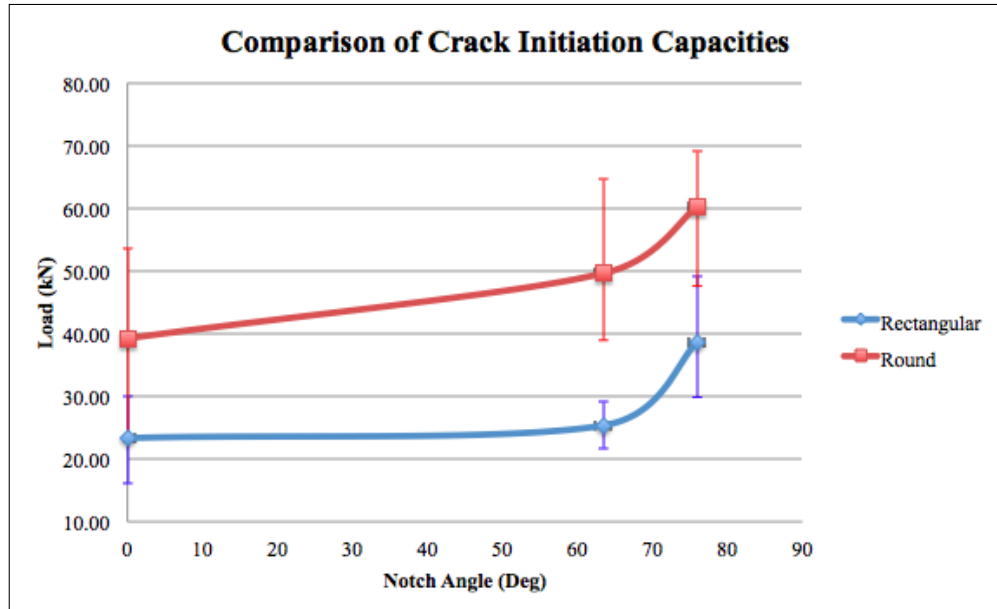


Figure 64: Comparison of rectangular and circular section notch capacities

4.4 Predicted Capacities using Standards

4.4.1 AS1720 Notch Design

Using AS1720 design equation for rectangular section specimens, the graph shown in Figure 65 was established; which compares the design capacities predicted and the actual capacities of each notch slope. The green solid bars show the estimated capacities of the notches using a f'_{sj} of 4.2 for an S3 grade timber, and the error bars show the variance in the estimated results ranging from S2 to S5 grade timber. The safety factor (ϕ) was not incorporated in calculating the notch capacities. The other solid bars show the average results, calculated using the left hand side of the design Equation 2.4.1, with the M^* and V^* occurring at the notch corner in relation to the load at which the notch cracks (purple) and ultimate load (red) for the rectangular specimens.

From this graph, it is observed that the predicted capacities increase with an increasing notch angle as do the crack initiation and ultimate capacities. However, there is an order of magnitude difference between the theoretical and crack initiation capacities, and the difference between the theoretical and ultimate capacity is almost double that for the crack initiation for the 1:0

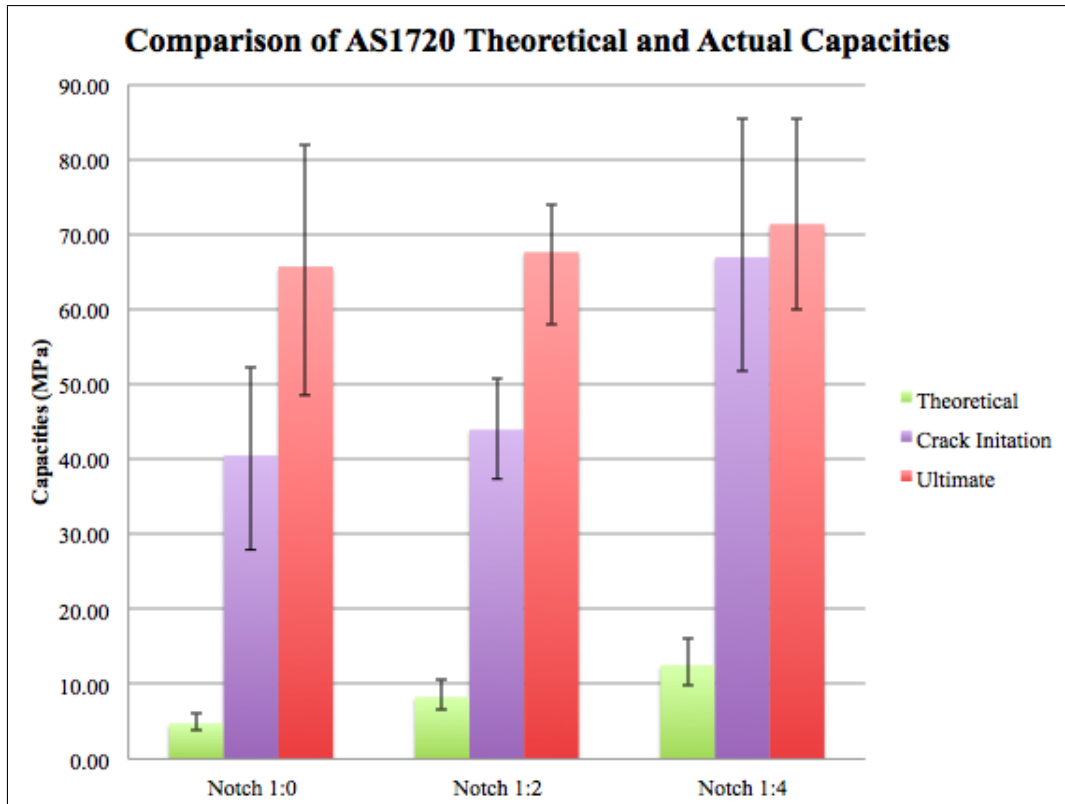


Figure 65: Comparison of AS1720 notch design capacities with experimental results

and 1:2 slopes. For this reason, it is assumed that the crack initiation load is considered as the point at which the notch fails, and is the capacity that this method is attempting to design for. The theoretical to notch initiation capacity ratios for this design method are 0.12, 0.19 and 0.19 for a 1:0, 1:2 and 1:4 slope notch respectively. Even though this method accounts for the increase in notch capacity through the increasing notch slope, from these results, this method is deemed inaccurate at estimating the capacity of the notch. The reason this design method yielded unsatisfactory results is assumed to be due to the assumption that timber is linearly elastic, made in derivation for this method. A further limitation of this method is it is purely designed for a rectangular section specimen and there is no obvious way to alter the design equation to accommodate a different beam section.

4.4.2 Eurocode 5 Notch Design

The standard European notch design equation in Eurocode 5, see Equation 2.4.4, was used to determine a theoretical shear stress at the notch corner as per the right hand side of the equation, for the rectangular specimens. This can be seen in Figure 66, where the theoretical capacity determined is compared to the actual shear stress (τ_d) at which the notch crack initiated. The green bar in the graph represents the theoretical capacity, calculated using a timber strength

class D40 for Eucalyptus trees. The corresponding error bars show the range in results using a D60 to D30 class, which correlate with Australian standard S2 to S5 classes. The other bars show the average shear stress at crack initiation (purple) and ultimate failure (red), and the error bars show the variance in the experimental results.

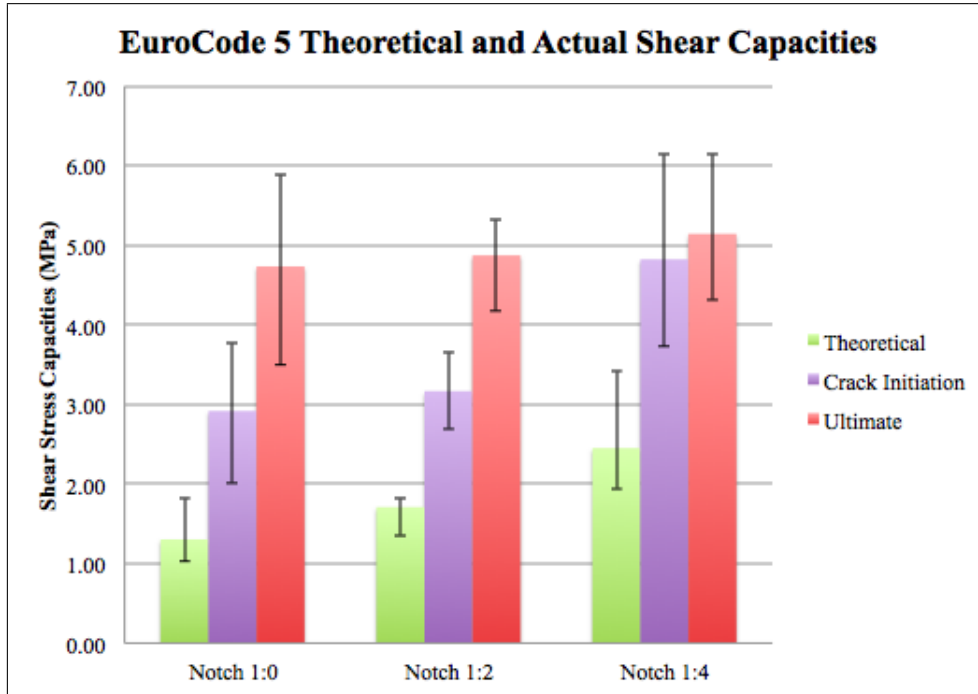


Figure 66: Comparison of Eurocode 5 notch design capacities with experimental results

It can be observed from Figure 66 that theoretical results and actual results follow a similar trend, where the capacity increases with an increasing notch slope. The same observation is made as for the AS1720 notch design, where it appears the design method is calculating the capacity at which the notch crack initiates, due to the large difference between ultimate and design capacities. The ratio of the theoretical and crack initiating capacities are determined to be 0.45, 0.54 and 0.51 for a 1:0, 1:2 and 1:4 notch slope respectively. This ratio shows the Eurocode notch design method is relatively accurate, with a factor of safety of around 0.5 for all notch slopes. The only limitation to this method is it only designs for a rectangular section specimen.

4.4.3 CSA O.86 Notch Design

The graph shown in Figure 67 was established to compare the CSA O.86 notch design method to the actual results gained through experimentation. The green bar shows the calculated notch resistance for sawn lumber under wet service conditions, excluding the safety factor (Φ). This

resistance can be compared to the average shear force at the notch corner, relating to the load at which the notch crack initiated (purple) and ultimate failure occurred (red). Due to the large difference between the theoretical capacity and the ultimate shear force, it is deduced that this design method is intending to calculate the shear force at the notch corner, related to the crack initiation load. It can be seen from this graph that this design method is inaccurate, having a very low theoretical to notch initiation capacity ratio of 0.17 for a rectangular specimen of 1:0 notch slope. This method also has a major limitation, where it does not account for a change in notch slope and only designs for a rectangular section. If this same capacity is compared to the 1:2 and 1:4 notch slope results, a theoretical to actual ratio of 0.16 and 0.11 are achieved respectively. Thus it is determined that this method was not accurate in calculating the notch capacity for the tested specimens.

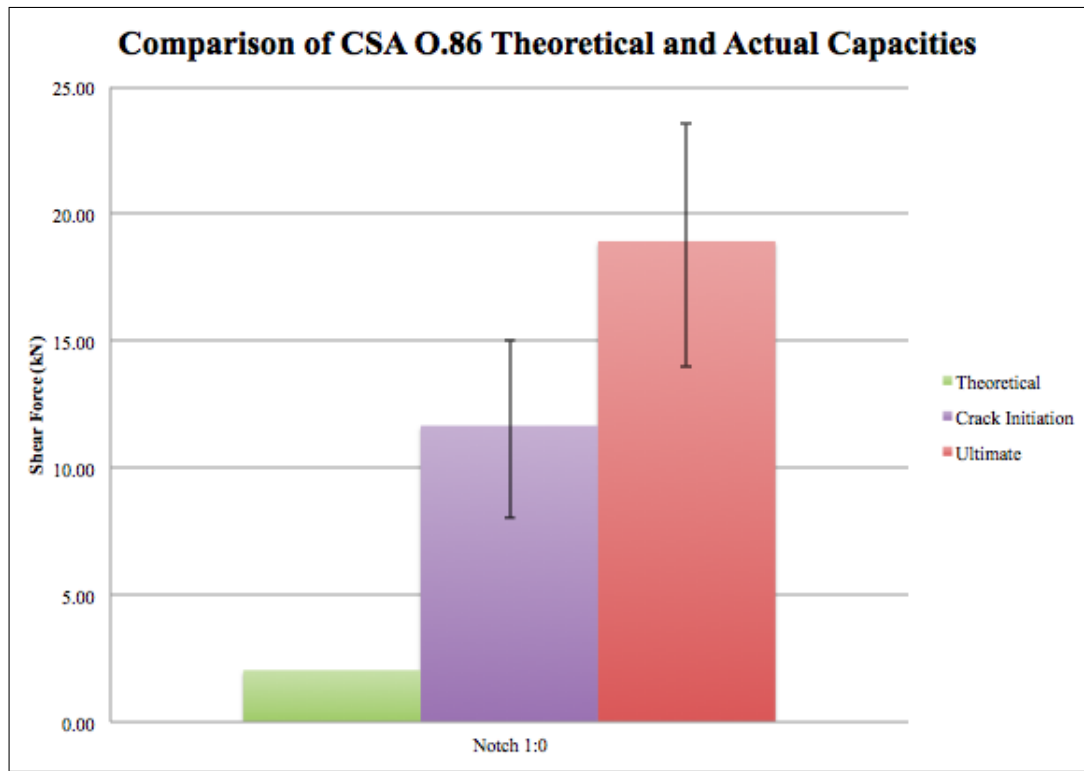


Figure 67: Comparison of CSA O.86 notch design capacities with experimental results

4.4.4 AS1720 Ultimate Section Design

Shear For a circular section, the equation to determine the ultimate design shear load (V_d) is shown in Equation 4.4.1

$$V_d = \phi k_1 k_4 k_6 k_{20} f'_s A_s \quad (4.4.1)$$

and the same equation applies for a rectangular section, accept it does not incorporate the factor k_{20} . After considering the shear equation given for both the rectangular and circular section, as well as general equations in determining shear force, it was established that the shear area can be found using,

$$A_s = \frac{It}{Q} \quad (4.4.2)$$

where

I = Moment of Inertia

Q = Statical Moment of Area

t = Thickness in Material Perpendicular to Shear

With this generalised equation for the shear area, an ultimate shear design load can be established for any cross-section. Thus, a design method can be established for a end notched specimen, using the cross-section over the notch. The following equations were established for the truncated, circular section over the notched end.

$$I_{notch} = \pi R^2 \left[\left(\frac{4R}{3\pi} \right)^2 + k^2 \right] - \frac{R^4}{8} \left[m + 2 \sin(2\theta) \sin^2(\theta) \right] + \frac{R^2 mk}{2} \left[\frac{8R \sin^3(\theta)}{3m} - k^2 \right] + 2R^4 \left[\frac{\pi}{8} - \frac{8}{9\pi} \right] \quad (4.4.3)$$

where

I_{notch} = Depth of notch

d = Depth of notch

R = Radius

$k = R - d$

$\theta = \arccos(k/R)$

$m = 2\theta - \sin(2\theta)$

The thickness in perpendicular to the shear load (t) and the statical moment of area (Q_{notch}) for the notched area are as follows,

$$t = 2\sqrt{R^2 - (\bar{y}_{notch} - k^2)} \quad (4.4.4)$$

$$Q_{notch} = A_{notch} \times \bar{y}_{notch} \quad (4.4.5)$$

with a total cross sectional area above the notch (A_{notch}) and vertical centroid (\bar{y}_{notch}) are given by

$$A_{notch} = \frac{R^2}{2}(2\pi - m) \quad (4.4.6)$$

$$\bar{y}_{tot} = k + \frac{4R}{3(2\pi - m)} \sin^3(\theta) \quad (4.4.7)$$

Using these equations in conjunction with Equations 4.4.2 and 4.4.1, an ultimate design shear load was established for the specific specimen, of 100mm diameter and 25mm deep notch, to be approximately 20.0kN, without a factor of safety (ϕ). All k values were taken as 1.0 accept k_{20} which was taken as 0.9, and f'_s was 5.0 MPa for F22 grade timber. Similarly, using the standard design equation specified for a rectangular section, a design shear load was determined for the rectangular notched section to be 14.0kN, not factored for safety. This was calculated for a 60mm width and 70mm depth over the notch, using the same k and f'_s as for the circular notched section. Figure 68 shows a comparison between the theoretical shear capacities calculated using this design method, with the actual ultimate shear capacities found through testing.

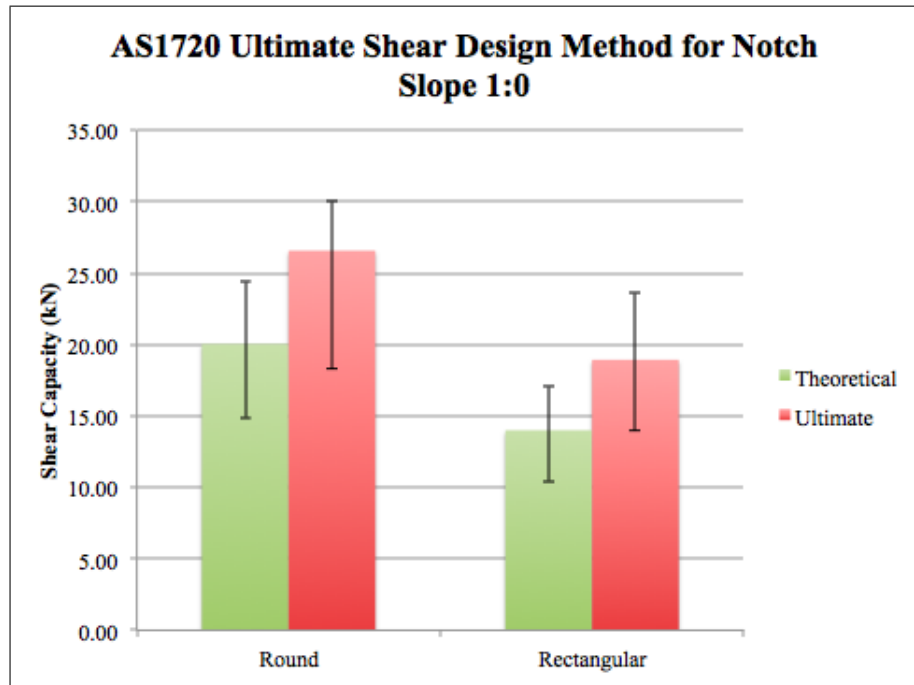


Figure 68: AS1720 ultimate shear design capacities compared to experimental results

The red bars represent the average ultimate shear capacity, with the error bars showing the variance in the results, and the green bars show the calculated capacity for F22 grade timber

and the error bars shows the variance for S2 and F14 grades. Figure 68 shows the calculated capacities are relatively accurate, showing a similar variance in error between the theoretical and actual results, and an average difference in capacities of 6.5kN for the round specimens and 4.9kN for the rectangular. From these results, a ratio of the theoretical and ultimate capacity was determined to be 0.75 for the round specimens and 0.74 for the rectangular specimens, which shows this method gives relatively accurate design capacities. Although, there is an issue surrounding this method, as it technically does not account for a notch with a sloped chamfer and only design for a 1:0 slope. However, when the same capacity is compared to the 1:2 and 1:4 shear capacities, a ratio of 0.68 and 0.65 respectively for a round specimen, and 0.72 and 0.68 respectively for a rectangular specimen. These theoretical to actual capacity ratios show the design capacities are still fairly accurate in accounting for a 1:2 and 1:4 chamfer in both sections. Overall this method was fairly accurate in designing for both specimens and all notch slopes, even though it is not modified to account for the extra strength supplied by a chamfer.

Bending

For a circular section, the equation to determine the ultimate design Moment (M_d) is shown in Equation 4.4.8

$$M_d = \phi k_1 k_4 k_6 k_9 k_{12} k_{20} k_{21} k_{22} f'_b Z \quad (4.4.8)$$

and the same equation applies for a rectangular section, accept it does not incorporate the factor k_{20} to k_{22} . To establish a method in designing for the ultimate bending moment for a circular notched beam, the section modulus for the truncated notched section can be used in the design equation. Equation 4.4.9 gives the section modulus for the notched circular section.

$$Z = \frac{R^4}{R + k + \bar{y}_{tot}} \left(\alpha - \sin(\alpha) \cos(\alpha) + \sin^3(\alpha) \cos(\alpha) - \frac{16 \sin^6(\alpha)}{9(\alpha - \sin(\alpha) \cos(\alpha))} \right) \quad (4.4.9)$$

Using these equations, a design bending capacity was established for the circular specimen as well as the rectangular specimen. A comparison of these estimated capacities to the experimental results can be seen in Figure 69.

The green bars in Figure 69 represent the capacities calculated using the standard moment design for an F22 grade timber, without incorporating a factor of safety (ϕ). The corresponding error bars show the variance in the estimated capacities for a range from F27 to F14 grade

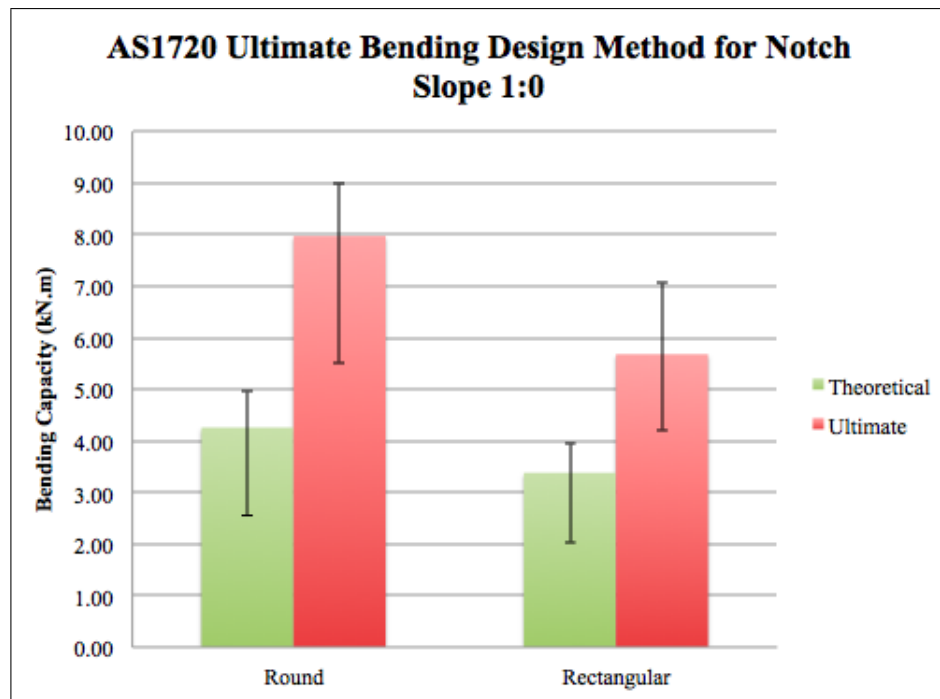


Figure 69: AS1720 ultimate bending design capacities compared to experimental results

timber. Overall this graph shows the calculated bending capacities using this method are fairly accurate, with a theoretical to ultimate capacity ratio of 0.53 for the round specimens and 0.59 for the rectangular. This method does have the same limitation as the shear, where it is only considering the truncated cross-section and does not account for a notch chamfer. However, when compared to the average experimental results for a 1:2 and 1:4 notch, the same calculated capacity achieves a ratio of 0.48 and 0.46 respectively, for the round specimen, and 0.58 and 0.55 respectively for the rectangular specimen. Thus the bending capacity is still fairly accurate for all notched specimens, although not as precise as the design shear capacity.

4.4.5 Comparison of Design Methods

To compare the overall design methods, the ratios of the theoretical capacities to the actual capacities for each method was graphed, shown in Figure 70. The closer these ratios are to 1.0, the more accurate the method is. All the results shown in this graph are for the rectangular specimen only, and the same theoretical capacity is compared to all notch slopes for the methods that don't design account for them.

When compared, it is deduced that AS1720 notch design and CSA O.86 yielded inaccurate results for calculating the experimental capacities, obtaining below 20% accuracy. Whereas Eurocode achieved roughly 50% accuracy and AS1720 ultimate design obtained around 70%

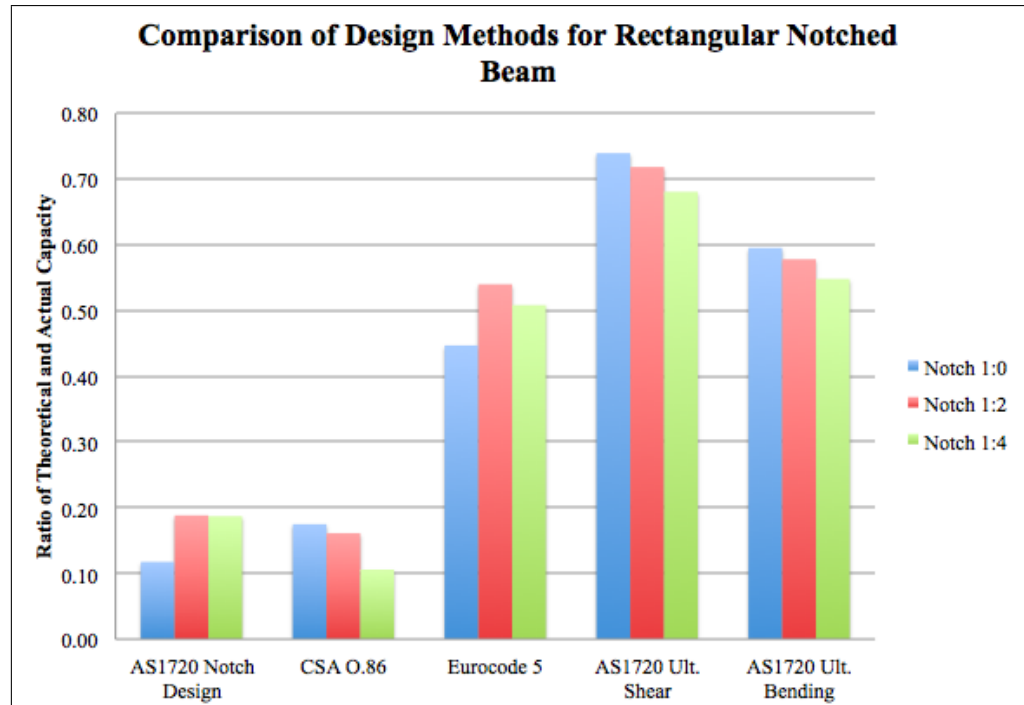


Figure 70: AS1720 ultimate bending design capacities compared to experimental results

accuracy for shear and below 60% for bending. The reason AS1720 notch design yielded unsatisfactory results is most likely due to the method's assumption that timber is a linearly elastic material. As for CSA O.86, the reason this method obtained inaccurate results is unknown, as it is based on the same fracture mechanics equation, derived by Gustafsson, as Eurocode design. However, when the design equations are compared, it can be seen that CSA design significantly modifies Gustafsson's original equation, whereas Eurocode does not. Overall, the optimal design method in accordance with these experimental results was AS1720's ultimate design for shear and bending, using the cross section over the notch. However, as this method does not account for the a notch slope and is purely based on ultimate failure, it is determined that Eurocode 5 design was optimum in designing for notch failure for rectangular specimens.

The only design method that designs for a notched round specimen is the modified AS1720 ultimate design in shear and bending, which achieved an accuracy of 75% for shear and 53% for bending.

5 Conclusions

1. The critical notch slope, which yielded the lowest member capacities, was found to be a slope of 1:0 for both rectangular and round specimens. Whereas a notch slope of 1:4 was found to obtain the highest member capacities for both sections, complying with recommendations from AS1720 and Department of Transport and Main Roads to use this notch slope in timber bridges.
2. Notch crack growth was found to be more brittle and sudden in the rectangular specimens than the round; which showed a more gradual crack growth. This was assumed to be due to the differing fibre arrangement between the rectangular and round specimens.
3. The ultimate failure modes differed between the two section members, where the rectangular members consistently failed in shear and the round predominantly failed in flexure. The cause of this was assumed to be due to a combination of the differing fibre arrangement between the two sections, and the round section having a larger area above the notch corner than the rectangular section.
4. The optimal design method was determined to be AS1720 ultimate design for shear and bending, using section above the notch. This method was also modified to account for the circular section, thus obtaining a method for designing notched round members. However, this design method only accounted for the ultimate failure of the beam, thus it was determined that the optimal method of designing for the crack initiation capacity was Eurocode 5 design.

6 Recommendations

The results from this thesis established a better understanding of how notched rectangular and circular beams react to loading. With this new information, it is recommended that further research be undertaken into determining methods of strengthening these notches, particular the critical 1:0 slope notch. It is also suggested that design methods for octagonal notched beams be derived and studied, as there is no current design method for this section, and they are commonly used throughout timber bridge construction. The combination of an optimal method in designing notched beams for all sections, alongside the determination of an effective method of strengthening notches, would severely increase the lifespan of many timber bridges currently in use.

References

- [1] Department of Transport and Main Roads . Timber bridge maintenance manual, February 2005.
- [2] Kym Wilkinson. *Capacity evaluation and retrofitting of timber bridge girders*. PhD thesis, Queensland University of Technology, 2008.
- [3] Section 8: Preservative and Protective Treatments. In *Timber Bridge Manual*. NSW Government, 1st edition edition, 2008.
- [4] Michael A. Ritter. *Timber bridges: design, construction, inspection, and maintenance*. Washington, DC, 1990.
- [5] Elizabeth Dunningham and Rosie Sargent. Review of new and emerging international wood modification technologies. *Forest & Wood Products Australia*, 2015.
- [6] Judith J. Stalnaker. *Structural Design in Wood*. Springer Science & Business Media, April 2013.
- [7] Lesley Cresswell, Jon Attwood, Alan Goodier, and Barry Lambert. *Product Design Graphics with Materials Technology*. Heinemann, second edition, 2004.
- [8] Amar K. Mohanty, Manjusri Misra, and Lawrence T. Drzal. *Natural Fibers, Biopolymers, and Biocomposites*. CRC Press, April 2005.
- [9] Alessio Pipinato. *Innovative Bridge Design Handbook: Construction, Rehabilitation and Maintenance*. Butterworth-Heinemann, November 2015.
- [10] Chris Marshall and Philip Schmidt. *Black and Decker The Complete Guide to Basic Woodworking: Skills and Projects Every Woodworker Needs*. Creative Publishing International, February 2005.
- [11] Softwood Material Science for Furniture SMEs and Designers, 2016.
- [12] Anatole A. Klyosov. *Wood-Plastic Composites*. John Wiley & Sons, October 2007.
- [13] RTA. Timber Beam Bridges, 2000.
- [14] *Queensland Agricultural Journal*, volume Volume 5. Hon. Secretary For Agriculture, 1899.
- [15] David L. Harrowfield. Analysis of timber weathering and wind velocity at Cape Adare, with comments on other historic sites in Antarctica. *Polar Record*, 42(04):291–307, 2006.

- [16] Kenneth White. *Bridge maintenance inspection and evaluation*, volume 9. CRC Press, 1992.
- [17] R. O. Heckrodt. *Guide to the Deterioration and Failure of Building Materials*. Thomas Telford, 2002.
- [18] M. J. Ryall. *Bridge Management*. Elsevier, 2001.
- [19] Sven Thelandersson and Hans J. Larsen. *Timber Engineering*. John Wiley & Sons, March 2003.
- [20] Nikolaos Plevris and Thanasis C. Triantafillou. FRP-reinforced wood as structural material. *Journal of materials in Civil Engineering*, 4(3):300–317, 1992.
- [21] Ibrahim M. Mahdy Bazan. Ultimate bending strength of timber beams. 1980.
- [22] Andrew H. Buchanan. Combined bending and axial loading in lumber. *Journal of Structural Engineering*, 112(12):2592–2609, 1986.
- [23] Juliano Fiorelli and Antonio Alves Dias. Fiberglass-reinforced glulam beams: mechanical properties and theoretical model. *Materials Research*, 9(3):263–269, September 2006.
- [24] Lorraine Joseph Markwardt and Thomas Randall Carson Wilson. *Strength and Related Properties of Woods Grown in the United States*. U.S. Government Printing Office, 1935.
- [25] J. C. F. Walker, B. G. Butterfield, J. M. Harris, T. A. G. Langrish, and J. M. Uprichard. *Primary Wood Processing: Principles and practice*. Springer Science & Business Media, April 2013.
- [26] U. S Department of Agriculture. *The Encyclopedia of Wood*. Skyhorse Publishing Inc., 2007.
- [27] Jack Porteous and Abdy Kermani. *Structural Timber Design to Eurocode 5*. John Wiley & Sons, April 2013.
- [28] Robert Jockwer, Rene Steiger, and Andrea Frangi. State-of-the-Art Review of Approaches for the Design of Timber Beams with Notches. *Journal of Structural Engineering*, 140(3), 2013.
- [29] Robert Jockwer. *Structural behaviour of glued laminated timber beams with unreinforced and reinforced notches*. PhD thesis, Diss., Eidgenossische Technische Hochschule ETH Zurich, Nr., 2014.

- [30] P. J. Gustafsson. A study of strength of notched beams. CIB W18-A, Meeting 21. Paper 21 – 10 – 1, 1988.
- [31] Erik Serrano, Per Gustafsson, Faculty of Engineering, LTH, Department of Construction Sciences, Byggnadsmekanik, Structural Mechanics, Institutionen for byggvetenskaper, Lunds universitet, Institutioner vid LTH, Lunds Tekniska Hogskola, Lund University, and Departments at LTH. Fracture mechanics in timber engineering – Strength analyses of components and joints. *Materials and Structures*, 40(1):87 – 96, January 2007.
- [32] *Eurocode 5: Design of Timber Structures*. European Standards, 1995.
- [33] H. Riberholt, B. Enquist, P. J. Gustafsson, and R. B. Jensen. *Timber beams notched at the support*. Afdelingen for Baerende Konstruktioner, Danmarks Tekniske Hojskole, 1991.
- [34] *CSA O.86:2014 Engineering Design in Wood*. CSA Group, Canada, 2014.
- [35] *Errata: Wood Design Manual*. The Canadian Wood Council, August 2013.
- [36] Ian Smith and Gerret Springer. Consideration of Gustafsson's proposed Eurocode 5 failure criterion for notched timber beams. *Canadian Journal of Civil Engineering*, 20(6):1030–1036, 1993.
- [37] R. H. Leicester. The size effect of notches. In *Proc., 2nd Australasian Conf. on Mech. of Struct. Mater., Melbourne*, volume 4, 1969.
- [38] Maha Fawwaz and Adnan Hanna. *Structural behavior of notched glulam beams reinforced by means of plywood and FRP*. PhD thesis, 2012.
- [39] Yail J. Kim and Kent A. Harries. Modeling of timber beams strengthened with various CFRP composites. *Engineering Structures*, 32(10):3225–3234, October 2010.
- [40] Roman Martin Elsener. *Material characterization of timber utility poles using experimental approaches*. PhD thesis, 2014.
- [41] Gary Hopewell. Spotted gumproperties and uses, November 2004.

Appendix A *Rectangular Specimen Characteristics*

Appendix B *Round Specimen Characteristics*

Appendix C *Strain Gauge Results*